

# **Deflectometric Measurement of Solar Concentrating Mirror Panels**

**Paul Scott u4216533**

Supervised by Greg Burgess

March 4, 2010

A thesis submitted in partial fulfillment of the degree of  
Bachelor of Engineering  
Department of Engineering  
Australian National University

This thesis contains no material which has been accepted for the award of any other degree or diploma at any other university. To the best of the author's knowledge, it contains no materials previously published or written by another person, except where due reference is made in the text.

Paul Scott, June 28, 2014

Thanks go out to my supervisor Greg for all his time I used up and help he gave me. Thanks also to all the staff out at the Solar Thermal Group, for covering the costs of the project and allowing me access to workshop space and tools.

As always thanks to all my family and friends for your understanding and the support.

Deflectometry promises to provide a fundamentally smarter approach to measuring the optical properties of solar concentrating mirrors. A method based on deflectometry was developed called Coloured Pattern Deflectometry (CPD), which measures the radii of curvature and slope errors for mirror panels made by the Solar Thermal Group at the ANU. The aim was to outperform currently used photogrammetry and flux mapping techniques.

The method agrees with photogrammetry to within 5% for radius of curvature measurements, for panels with a radius of curvature around 30m. The discrepancy is caused by a systematic error in the method, the source of which was not found.

CPD slope error measurements agree with those from flux mapping, but a different comparison is needed to check the accuracies.

The method is in a semi-useful state, with further testing and debugging the errors can be reduced so that the system becomes more practical.

# Contents

<b>1. Introduction</b>	<b>12</b>
1.1. Motivation . . . . .	12
1.2. Current Methods . . . . .	13
1.3. Thesis Outline . . . . .	14
<b>2. Background Theory</b>	<b>15</b>
2.1. Mirror Panel Radius of Curvature . . . . .	15
2.2. Slope Error . . . . .	18
<b>3. Literature Review</b>	<b>21</b>
3.1. Photogrammetry . . . . .	21
3.2. Flux Mapping . . . . .	23
3.3. Dial Gauge Measurements . . . . .	24
3.4. Deflectometry . . . . .	25
<b>4. Coloured Pattern Deflectometry</b>	<b>29</b>
4.1. Overview . . . . .	30
4.2. Reflected Light Vector . . . . .	31
4.3. Pattern Source Position . . . . .	34
4.4. Surface Position . . . . .	37
4.5. Simulation . . . . .	38
<b>5. Implementation</b>	<b>43</b>
5.1. Construction and Calibration . . . . .	43
5.1.1. Mirror Frame . . . . .	43
5.1.2. Coloured Pattern . . . . .	45
5.1.3. Camera Calibration . . . . .	48
5.2. Programming . . . . .	48
5.2.1. Design . . . . .	49
5.2.2. Operation . . . . .	50
<b>6. Experimental Methods</b>	<b>53</b>
6.1. CPD Procedure . . . . .	53
6.2. Photogrammetry Measurements . . . . .	55
6.3. Flux Mapping Measurements . . . . .	55
6.4. Dial Gauge Measurements . . . . .	56

*Contents*

<b>7. Results and Discussion</b>	<b>57</b>
7.1. RoC Comparisons . . . . .	57
7.2. Slope Error Comparisons . . . . .	59
7.3. CPD Systematic Error . . . . .	62
7.4. Sensitivity Analysis . . . . .	65
7.5. Improvements . . . . .	67
<b>8. Conclusion</b>	<b>69</b>
<b>Appendices</b>	<b>70</b>
<b>Appendix A. Mirror Panel Equations</b>	<b>71</b>
A.1. Depth to RoC Approximation . . . . .	71
A.2. Temperature Effects . . . . .	71
A.3. Offset Slope Error . . . . .	72
<b>Appendix B. Camera and Lens Optics</b>	<b>73</b>
B.1. Lens Cardinal Points . . . . .	73
B.2. Radial Lens Distortion . . . . .	74
B.3. Focusing on Mirrored Surface . . . . .	75
<b>Bibliography</b>	<b>77</b>

# List of Figures

1.1.	ANU second generation parabolic dish. . . . .	12
1.2.	Stack of mirror panels in workshop. . . . .	13
2.1.	Arc lengths, tangent vectors and tangential angles marked at two points on a curve. The radius of curvature is marked for the first point on the curve. . . . .	15
2.2.	Surface intersected by orthogonal planes on which the principal curvatures lie. In the right hand image the curve of intersection has been highlighted, along with one principal radius of curvature for the point. . . . .	16
2.3.	Principal RoCs that best describe overall shape of mirror panel. . .	17
2.4.	Cross section of mirror panel. Slope error describes any local deviations from the fitted surface (dashed line). . . . .	18
2.5.	A simple surface translation has a minimal effect on the optics of a concentrating mirror, compared to a slope deviation. . . . .	18
2.6.	Real and ideal surface normals. . . . .	19
3.1.	A concentrating trough with reflective target points placed on it ready for measurement (Pottler et al. 2005). . . . .	22
3.2.	Measurement dots projected onto back of mirror panel (Burgess et al. 2009). . . . .	22
3.3.	Flux mapping a mirror panel. The superimposed paraboloid is the ideal surface for which slope errors are calculated. It has its focal length $f$ lined up with the incoming sun rays. . . . .	23
3.4.	Flux distribution of a mirror panel's focused spot. . . . .	24
3.5.	Dial gauge measurement being performed by STG staff member. . .	25
3.6.	Proposed deflectometry setup (Kammel & Puente León 2005). Intensity pattern on screen reflects off the surface to be measured into camera lens. . . . .	25
3.7.	Measurement taken of car door showing defects (Kammel & Puente León 2005). . . . .	26
3.8.	Potential setup of QualiSURF system (from <i>QualiSURF-R: Solar Applications</i> broacher, EOS Technologies Inc.). . . . .	27
3.9.	Setup of color-coded dish measurement system (Ulmer et al. 2008). . . . .	27
4.1.	Position vectors (pink) and surface normals (blue) for 3 points on a surface. . . . .	29

## List of Figures

4.2. Basic measurement setup. The path of a light ray originating on the pattern surface is shown, as it reflects off the mirror into the camera. . . . .	30
4.3. Different mirrored surfaces can reflect the same pattern source point into the same camera pixel. This means that there is an infinite number of mirror surfaces which could produce identical results in camera. . . . .	31
4.4. The lens and sensor array of a digital camera. Shown are 3 of the many paths light can travel from a point in focus, to its corresponding pixel in the camera array. The principal distance is the distance along the optical axis from the principal point to the sensor array. . . . .	32
4.5. Global coordinates and 3 reference dots positioned around mirror. Note that dot 2 does not necessarily lie along the y axis, but it is in x-y plane. . . . .	33
4.6. Target pattern colour gradient. . . . .	34
4.7. Measurement setup with a horizontally aligned pattern. A perpendicular view of the pattern is given showing lines of potential source points for a green light ray. . . . .	35
4.8. Measurement setup with a vertically aligned pattern. A perpendicular view of the pattern is given showing lines of potential source points for an orange light ray. . . . .	35
4.9. Silhouette of pattern with source lines superimposed. Potential source points are given by blue dots. . . . .	36
4.10. Reflection of two points on pattern surface into neighbouring camera pixels. . . . .	37
4.11. Two surface points corresponding to two neighbouring pixels in the camera. The surface position and slope of the first point is known. . . . .	38
4.12. Model setup. . . . .	39
4.13. Error between measured surface and fitted curve. . . . .	40
4.14. Slope errors calculated relative to fitted surface. . . . .	41
4.15. Difference between measured curve and actual curve, for the second set of parameters in table 4.1. . . . .	41
 5.1. Deflectometry setup. Mirror frame is on the left and the coloured pattern on the right. . . . .	43
5.2. Frame for holding mirror panel. Red highlights the 3 reference dots, yellow the mirror locating disk and blue the panel clamp. . . . .	44
5.3. Close up of the locating disk. The plane of the top left corner of the mirror panel is lined up with the plane of the locating disc. . . . .	44
5.4. One of the photogrammetry images for the mirror frame. . . . .	45
5.5. Back of coloured pattern showing frame. The blue area highlights the bearings and shaft holding coloured pattern. Orange highlights the locking pin used to hold the pattern in place. . . . .	45
5.6. Coloured pattern being rotated. . . . .	46

## List of Figures

5.7.	Up close photograph of printed colour pattern. A segment transitions from red at $H = 0.0$ , through yellow, green, blue, purple and then back to red at $H = 1.0$ . . . . .	46
5.8.	Pixel hue plotted against pixel position within segment, for cool-white fluorescent camera setting. Curves are shown at different segment illuminations. The overlap of the curves indicates a good level of reproducibility. . . . .	47
5.9.	Zoomed in section of pattern segment demonstrating vertical pairing. The top image is a TIFF and the bottom is a RAW image. Hues are given for some pixels with values in the range of $0 \rightarrow 255$ . . . . .	48
5.10.	Interaction of source files. Upper list is a file's parameters, and lower is its functions. A + indicates that the parameter/function is to be used external to the file, while a - indicates it is internal. An arrow pointing at a file indicates its functions and/or parameters are being used by file at base of arrow. . . . .	50
6.1.	Taking photograph of mirror panel surface. Top left corner of mirror panel is lined up so that it reflects the top right corner segment of the coloured pattern, as marked on image by green line. . . . .	53
6.2.	Orange plastic placed over fluorescent light to change the lighting colour of the workshop. . . . .	55
7.1.	A mirror panel has its edges labelled like a compass. Here the mirror panel ID label is on the back surface, at the bottom. $\phi$ is the rotation of the principal direction $R_1$ , relative to the E-W mirror axis. . . . .	57
7.2.	Plot of principal RoCs for mirror panels measured with both deflectometry and photogrammetry. . . . .	59
7.3.	3D mesh of panel 210906 surface, with highly exaggerated z axis in mm. The closest corner is the top left corner of the mirror panel as it was measured. The edges of the panel can be seen to spring back from the rest of the panel shape which is an artefact of manufacturing process. . . . .	60
7.4.	Slope error plot for panel 035 with x component on left, and y component on right. . . . .	61
7.5.	Slope error plot for panel 210906 with x component on left, and y component on right. . . . .	61
7.6.	Panel 411 (left) and 015 difference surfaces relative to photogrammetry. Note that the x and y axes correspond to bin numbers. . . .	63
7.7.	Panel 411 difference surfaces. Left plot was measured with t orientation, centre plot with l orientation, and right plot with r orientation. . . .	63
7.8.	Panel 411 difference surfaces. Left plot uses the top left as a starting point, the centre plot uses top right, and the right plot uses the centre of the panel. . . . .	64

*List of Figures*

A.1. Relationship between the depth of a spherical mirror panel and its RoC. . . . .	71
A.2. Relationship between the depth of a spherical mirror panel and its RoC. . . . .	72
B.1. Optical axis of a simple convex lens. Rays striking the lens will be refracted if they aren't on the optical axis. . . . .	73
B.2. Focal points of lens. . . . .	74
B.3. Camera focused on mirrored surface. . . . .	75
B.4. Camera focused on coloured pattern. . . . .	76

# List of Tables

4.1.	Simulation results. . . . .	39
6.1.	Camera settings. . . . .	54
7.1.	RoC results. * Photogrammetry was performed on front of panel. † 4 point dial gauge measurement. Suffix of deflect corresponds to the orientation of the panel as it was measured: b-bottom, t-top, l-left, r-right. . . . .	58
7.2.	Slope error results for mirror panels. . . . .	60
7.3.	Measurements taken at different panel orientations. Suffix of deflect corresponds to the orientation of the panel as it was measured: b- bottom, t-top, l-left, r-right. . . . .	62
7.4.	Results for different panel 411 surface starting points. T-top, B- bottom, L-left, R-right, M-middle. . . . .	64
7.5.	Percent change in deflectometry measurements, for changed mea- surement setup. . . . .	65
7.6.	Percent change in panel 411 deflectometry results, for change in parameters. . . . .	67

# 1. Introduction

## 1.1. Motivation

Solar concentrators are proving to be an important renewable energy technology, that will likely generate a significant proportion of the world's future energy needs. As in many areas of engineering, there is a constant need to produce more efficient concentrator designs. Greater efficiency is often achieved by increasing the intensity of the focused light. In reflective concentrators, one way of increasing the intensity of the focused light, is to improve the optical performance of the mirrored surfaces. Therefore it is crucial to have a method of measuring the optical properties of the mirrored surfaces.



Figure 1.1.: ANU second generation parabolic dish.

The second generation SG4 dish, developed by the Solar Thermal Group (STG) at the Australian National University (ANU), is a  $500\text{m}^2$  paraboloidal concentrator (figure 1.1). The reflecting surface of SG4 is made up of 380 identical  $1.2\text{m} \times 1.2\text{m}$  square segments called mirror panels (also known as mirror facets). To produce the best performance, the curvature of each mirror panel would match the local curvature of the underlying paraboloidal shape. However, to reduce complexity and costs, SG4 was designed to be made from mirror panels that all have the same curvature (Johnston et al. 2003). The mirror panel curvature was chosen so that on average it gives the best approximation to the paraboloidal dish curvature.

It is important to measure the curvature of each panel as it is made, to ensure that it meets the set target. In practice, the mirror panel manufacturing process produces panels with a range of curvatures about the target curvature. In most cases these non conforming panels are still used. If placed on a section of the dish

## 1. Introduction



Figure 1.2.: Stack of mirror panels in workshop.

where they best match the local paraboloid, these panels can even improve the dish optics.

Another important quantity to measure is the slope error of a mirror panel. Slope error uses a statistical distribution to represent all the small imperfections deviations in a mirror panel surface. As well as providing a general indication of mirror surface quality, it can also be used to model the resulting flux at the focus of a dish.

Curvature and slope error are also important quantities to measure for the mirror panels (facets) used in other concentrators, such as heliostats, Fresnel systems and troughs.

## 1.2. Current Methods

The STG currently employs 3 different techniques to measure mirror panels. Each technique is limited in one way or another, so a combination of techniques is often used to get detailed information. The first of these, photogrammetry, provides information on panel curvatures, but only limited information on panel slope errors. This process is time consuming and requires the mirror panel surface to be painted for the most accurate results (Burgess et al. 2009).

The second technique, flux mapping, gives reasonable slope error information, but no accurate curvatures for a mirror panel. It is also a time consuming process which can only be performed on a sunny day at low sun elevations.

The final process is dial gauge measurements which are simple and reasonably fast to perform. However they only produce unreliable curvature data.

An ideal mirror panel measurement system used in research and manufacturing would meet the following requirements:

1. Provide curvatures
2. Provide slope errors
3. Accurate and reliable

## *1. Introduction*

4. Simple to operate
5. Fast
6. Cheap to set up
7. Compact

Any one of the currently used methods do not adequately fulfil all these needs. It is likely that with enough process design, photogrammetry could adequately meet all these requirements. However there is a fundamentally better approach for making the required measurements. This approach uses a technique known as deflectometry.

Fundamentally deflectometry systems measure surface slopes accurately while triangulation techniques such as photogrammetry measure surface positions accurately (Kammel & Puente León 2005). For concentrating mirror applications surface slopes are the more important quantity to measure. This is because a small change in mirror slope can have a much greater effect on the optics than a small change in mirror surface position.

Deflectometry is well established in the car manufacturing industry for providing quality checks on painted surfaces and glass. Recently effort has gone into applying it to solar concentrators such as troughs and whole dishes. A little research has been also done on applying deflectometry to mirror panels and facets, but nothing specifically tailored for the mirror panels produced by the STG at the ANU.

### **1.3. Thesis Outline**

This thesis aims to develop a STG mirror panel measurement technique based on deflectometry. This technique will be simple and quick to use, cheap to set up and provide information on slope errors and curvatures with errors similar to, or better than those of the current methods.

This method will simplify the act of characterising mirror panels. In manufacturing this will save costs and allow greater control of panel quality. In the area of concentrator research, it will potentially allow more detailed temperature deflection and life-cycle analysis.

In order to achieve this goal, the first task was to review the current literature on deflectometry (chapter 3). The second step was to develop the theory behind a new deflectometry technique, to perform curvature and slope error measurements on mirror panels (chapter 4). This new technique was then implemented, by constructing the required measurement apparatus and programming the required software (chapter 5). The final steps to achieving the aim, were to run experiments on technique, and compare the results with independent measurements (chapters 6 and 7).

Before getting into this, the next chapter gives a background on the important mirror panel quantities of radius of curvature and slope error.

## 2. Background Theory

This chapter explains the concepts of radius of curvature and slope error, which describe the optics of a mirror panel. It is important to understand these terms from the start, since they are used extensively throughout the literature, and the rest of this thesis.

### 2.1. Mirror Panel Radius of Curvature

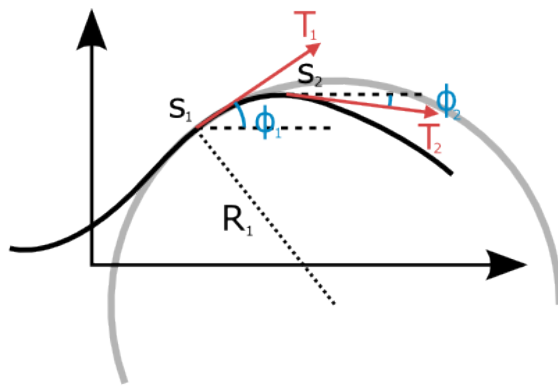


Figure 2.1.: Arc lengths, tangent vectors and tangential angles marked at two points on a curve. The radius of curvature is marked for the first point on the curve.

The curvature of a curve in 2D space (as shown in figure 2.1) is given by Weisstein (n.d.a):

$$\kappa = \frac{d\phi}{ds} \quad (2.1)$$

Where  $\phi$  is the curve tangential angle given by  $\tan(\phi) = \frac{y}{x}$  and  $s$  is the curve arc length. It can be thought of as the infinitesimal change in the direction of the curve tangent, for an infinitesimal change in position along the curve path.

The radius of curvature (RoC) for a point on a curve, is the radius of a circle which has the same curvature as that point. It is given by:

$$R = \frac{1}{|\kappa|} \quad (2.2)$$

## 2. Background Theory

A point on a 2D surface in 3D space can also have a curvature. A plane that contains a surface point and the point's surface normal, will form a curve where it intercepts with the surface. The curvature of this curve is known as one of normal curvatures for the given point. An infinite number of such normal curvatures can be calculated for a given point, by rotating the intercepting plane about the surface normal. Out of all these normal curvatures, the maximum and minimum are known as the principal curvatures  $\kappa_1$  and  $\kappa_2$ . The planes that two the principal curvatures lie in are orthogonal to one another (Weisstein n.d.*b*). The principal directions are the tangent directions of the principal curvatures.

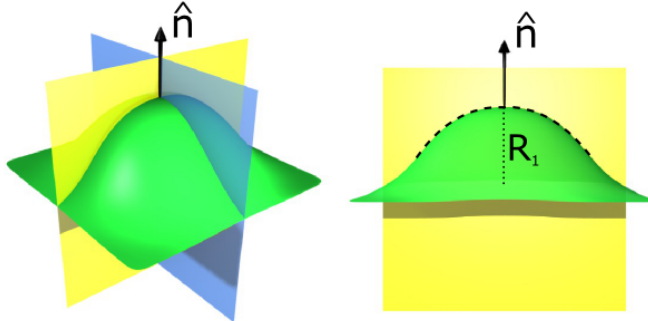


Figure 2.2.: Surface intersected by orthogonal planes on which the principal curvatures lie. In the right hand image the curve of intersection has been highlighted, along with one principal radius of curvature for the point.

The inverse of the principal curvatures are known as the principal radii of curvature  $R_1$  and  $R_2$ , where  $R_1$  is the larger of the two. The geometric mean radius of curvature is:

$$R_G = \sqrt{R_1 R_2} \quad (2.3)$$

For a dish mirror panel, we are only really interested in its overall curvature, not the local curvature at each point on the panel's surface. This is because the surface curvature of a parabolic dish does not change much over the length of one mirror panel, and the panels are meant to have a roughly spherical shape anyway (every point on the surface of a sphere has the same curvature). Therefore a mirror panel is described by the principal RoCs which best match its overall shape (see figure 2.3). Any local fluctuations in this curvature are considered to be slope errors, which are discussed in the section to follow.

One method of measuring a mirror panel's RoCs is to measure a set of points on the mirror surface, and then fit a function to these points. The parameters used to fit the function can then be used to calculate the panel's RoCs. For example a sphere may be fitted to a set of measured surface points, with the sphere radius as one of the fitting parameters. The optimal radius can be thought of as an average RoC for the panel, somewhere between the two principal RoCs.

## 2. Background Theory

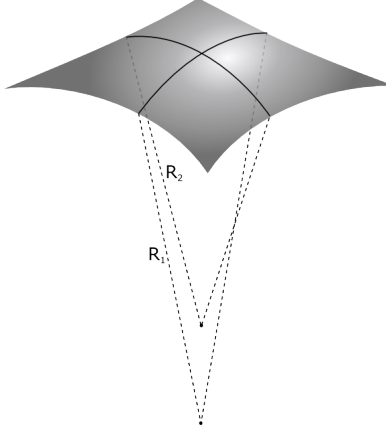


Figure 2.3.: Principal RoCs that best describe overall shape of mirror panel.

To measure the principal RoCs, a function is required that has orthogonal RoCs that can change independent of one another. A spheroid, ellipsoid or an elliptic paraboloid could be used for this task. In practice an elliptic paraboloid is used because it is mathematically simpler and provides a good fit to mirror panel data. An elliptic paraboloid is described by the equation:

$$z = \frac{x^2}{4f_x} + \frac{y^2}{4f_y} \quad (2.4)$$

Where  $f_x$  and  $f_y$  are the x and y focal lengths of the paraboloid. The curvature in the x-z plane is simply given by the curvature of a parabola:

$$\kappa_x = \frac{1}{2f_x(1 + \frac{x^2}{4f_x^2})^{3/2}} \quad (2.5)$$

At the origin ( $x = 0$ ) this gives the radius of curvature:

$$R_x = \frac{1}{|\kappa_x|} = 2f_x \quad (2.6)$$

Similarly, the radius of curvature in the y-z plane at the origin is:

$$R_y = \frac{1}{|\kappa_y|} = 2f_y \quad (2.7)$$

The curvature of a long focal length paraboloid does not change much over a distance equal to the size of a mirror panel. For example take the case where we have a paraboloid with a focal length of  $f_x = 15\text{m}$ . The radius of curvature at the origin will be  $R_x = 30\text{m}$ . If we move 0.6m (half the width of a mirror panel) out from the origin, the RoC in the x-z plane will be:

$$R = \frac{1}{|\kappa|} = 2 * 15 \left(1 + \frac{0.5^2}{4 * 15^2}\right)^{3/2} = 30.018\ldots\text{m} \quad (2.8)$$

## 2. Background Theory

This is only a tiny change in RoC over the length of a mirror panel. Therefore the principal RoCs of a mirror panel can be calculated by fitting to it an elliptic paraboloid, and then multiplying the paraboloid focal lengths by 2.

### 2.2. Slope Error

Slope errors are used to statistically accounting for the error between two surfaces. The RoCs discussed in the previous section describe the overall shape of a mirror panel. Slope errors can be used to describe the left over deviations between such a RoC best fit surface, and the actual surface. These deviations might be due to such things as local mirror deformations or aberrations in the mirror glass itself.



Figure 2.4.: Cross section of mirror panel. Slope error describes any local deviations from the fitted surface (dashed line).

These errors are represented in terms of surface slope errors instead of surface position errors, because slope differences have a greater impact on a reflecting optical system. To explain this consider the concentrating mirror in figure 2.5. In the first case a section of the mirror has been translated a small amount from its ideal position. This will give a high position error but it has a minimal effect on the mirror focus. In the second case a section of surface has a large slope error. This has a drastic effect on the reflected light, which completely misses the focus for the rest of the mirror.

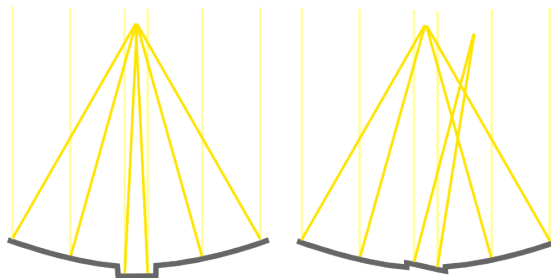


Figure 2.5.: A simple surface translation has a minimal effect on the optics of a concentrating mirror, compared to a slope deviation.

The slope error at a point on a mirror surface, is the deviation of its surface normal (slope), from the surface normal of an ideal shape. To illustrate this, consider the two surface normals in figure 2.6. These normals represent just one point on a mirrored surface. To simplify things local coordinates are used, with the z axis lined up with the ideal surface normal. The local x axis is kept in the global coordinate system x-z plane. This roughly positions the local y axis in the global y-z plane.

## 2. Background Theory

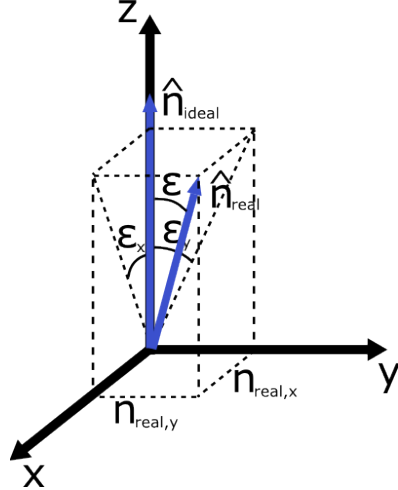


Figure 2.6.: Real and ideal surface normals.

The slope error  $\varepsilon$  is the angle that the real normal makes with the z axis. This slope error can be broken down into x and y components. The real normal projected onto the x-z plane makes an angle with the z axis. This angle is the x component of slope error  $\varepsilon_x$ . Similarly, projecting the real normal onto the y-z plane produces the y component of slope error  $\varepsilon_y$ . For small deviations from the ideal surface normal,  $\sin(\varepsilon_x) \approx \varepsilon$ , therefore the slope error components approximate to:

$$\varepsilon_x \approx n_{real,x} \quad (2.9)$$

$$\varepsilon_y \approx n_{real,y} \quad (2.10)$$

Johnston (1995) suggests that the slope error does not have to be split up into components as we have done here. However Burgess & Lovegrove (2007) have found that important information can be gained by using two angles instead of one.

The slope error at any given point on a mirror panel is close to random. As (Pettit 1977) and (Butler & Pettit 1977) have shown, this allows the slope errors of a whole mirror surface to be statistically represented by a bivariate Gaussian distribution. The probability of slope error components  $\varepsilon_x$  and  $\varepsilon_y$  occurring are then given by:

$$P_{\varepsilon_x \varepsilon_y} = \frac{1}{2\pi\sigma_{\varepsilon_x}\sigma_{\varepsilon_y}} e^{-\left(\frac{\varepsilon_x^2}{2\sigma_{\varepsilon_x}^2} + \frac{\varepsilon_y^2}{2\sigma_{\varepsilon_y}^2}\right)} \quad (2.11)$$

Where  $\sigma_{\varepsilon_x}$  and  $\sigma_{\varepsilon_y}$  are the standard deviations of the slope errors  $\varepsilon_x$  and  $\varepsilon_y$  respectively. They are calculated from:

$$\sigma_{\varepsilon_x}^2 = \sum_{k=1}^N \frac{(\varepsilon_{x,k} - \mu_{\varepsilon_x})^2}{N-1} \quad (2.12)$$

## 2. Background Theory

$$\sigma_{\varepsilon_y}^2 = \sum_{k=1}^N \frac{(\varepsilon_{y,k} - \mu_{\varepsilon_y})^2}{N - 1} \quad (2.13)$$

Where  $\varepsilon_{x,k}$  and  $\varepsilon_{y,k}$  are the x and y components of slope error for the  $k^{th}$  point on the mirror surface.  $\mu_{\varepsilon_x}$  and  $\mu_{\varepsilon_y}$  are the means of the respective slope error components.  $N$  is the total number of surface points.

Handling mirror panel slope errors in this manner, allows the use of statistical methods to predict the contribution of a mirror panel, to the intensity distribution at the dish focus. For further information on how this is done, see *Focal plane flux distributions produced by solar concentrating reflectors* by Harris & Duff (1981).

# 3. Literature Review

This chapter contains an overview of the more important mirror panel measurement techniques that are in common use at the STG. It then goes on to outline important research into deflectometry.

## 3.1. Photogrammetry

Photogrammetry is an accurate and reliable triangulation technique for measuring points in 3D space. It has a wide range of applications for solar concentrators and in other industries.

Pottler et al. (2005) explains the application of photogrammetry to solar concentrators in *Photogrammetry: A Powerful Tool for Geometric Analysis of Solar Concentrators and Their Components*. He gives high praise to the method in his abstract:

“Digital close range photogrammetry has proven to be a precise and efficient measurement technique for the assessment of shape accuracies of solar concentrators and their components. The combination of high quality mega-pixel digital still cameras, appropriate software, and calibrated reference scales in general is sufficient to provide coordinate measurements with precisions of 1:50,000 or better. The extreme flexibility of photogrammetry to provide high accuracy 3D coordinate measurements over almost any scale makes it particularly appropriate for the measurement of solar concentrator systems. It can also provide information for the analysis of curved shapes and surfaces, which can be very difficult to achieve with conventional measurement instruments.”

In photogrammetry a series of photographs are taken from different camera locations, of an object which has measurement points marked on it. These points are often dots that have been physically attached to the surface of the object, as has been done for the trough in figure 3.1. Every dot is uniquely identified in each photograph in which it is present. Reference dots with roughly known separations allow the position of the camera to be located in each photograph. A dot can be then be triangulated by working out its position in each photograph relative to the other dots and the camera.

Recently the STG at the ANU has been using photogrammetry to measure the shape of mirror panels as described in the paper *Photogrammetry for Dish Construction* by Burgess et al. (2009). They use the VMS (Vision Measurement

### 3. Literature Review

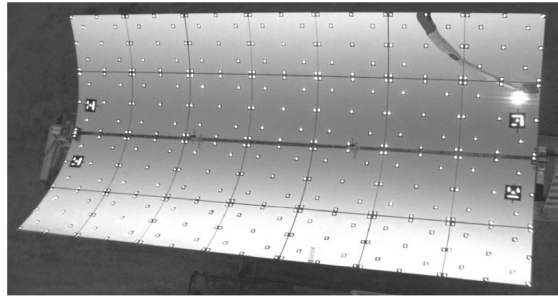


Figure 3.1.: A concentrating trough with reflective target points placed on it ready for measurement (Pottler et al. 2005).

System) Software, developed by Mark Shortis (RMIT) and Stuart Robson (University College London) to process the photographs. Instead of sticking hundreds of dots to each panel, they use a projector to project around 1829 dots onto the panel surface (see figure 3.2). This significantly speeds up the process, but the dots must be projected onto the non-reflective back of the panel, or the mirrored surface must be painted.

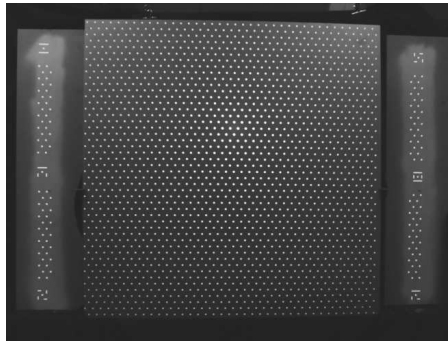


Figure 3.2.: Measurement dots projected onto back of mirror panel (Burgess et al. 2009).

27 photographs are taken of each panel. For a typical panel, photogrammetry solves point positions to within  $15\text{--}20\mu\text{m}$ , in the axis normal to the plane of the panel. They tested 3 panels to check the difference between taking measurements on the back of a panel and the painted mirror surface. They found a small systematic difference was found (within error bounds), that could be used to calibrate the rest of the panels.

It takes 15 – 20mins to measure and process the photogrammetry results for one panel, even when done as part of a batch of measurements.

More recently the STG has produced a way of constructing the surface slopes from the measured photogrammetry surface positions (Burgess, G., pers. comm., July 2009). This allows slope errors to be calculated. Initial experimentation has produced results that are comparable to flux mapping slope errors, however the method has large error bounds and a limited surface resolution.

### 3. Literature Review

## 3.2. Flux Mapping

Flux mapping is traditionally used to measure the performance of and to calibrate a complete concentrator. The concentrator is aimed at the sun, and a photograph is taken of the intensity (flux) distribution at the concentrator's receiver. The tighter the distribution the better the concentration. The concentrator can be optimized by observing changes in the distribution while altering things like receiver focal length and sun tracking. By comparing the resulting distribution with what would have resulted from an ideal concentrator surface, overall slope error values can be calculated for a concentrator.

*Novel Parabolic Trough Collectors Driving a Small-Scale Organic Rankine Cycle System* by Kohlenbach et al. (2007), describes the process of flux mapping a parabolic trough. The trough is aimed at the sun and a photograph is taken of the resulting flux distribution on a target placed at the focal plane of the trough.

The STG has been using flux mapping to measure the slope error and focal length of individual mirror panels. A mirror is used to focus the sun onto a flat white target surface as shown in figure 3.3. A photograph is taken of the resulting intensity distribution, which is then processed. A slope error is calculated by comparing the mirror panel to an ideal segment of a paraboloid, for the given sun angle and target distance. Ignoring the effect of the sun shape, such an ideal surface would focus to a single point. Therefore this slope error can be worked out by observing the intensity distribution of the focused spot, and removing the effects of sun shape on the flux distribution.

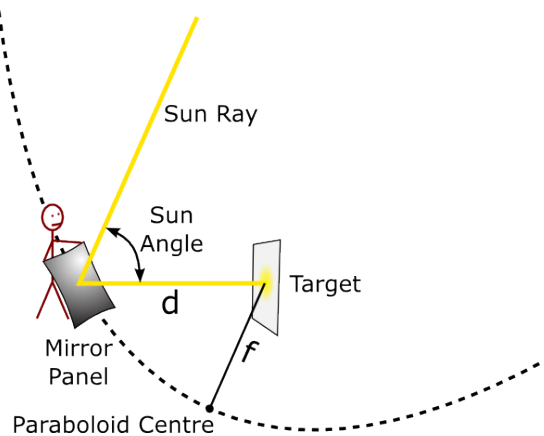


Figure 3.3.: Flux mapping a mirror panel. The superimposed paraboloid is the ideal surface for which slope errors are calculated. It has its focal length  $f$  lined up with the incoming sun rays.

The ideal paraboloid (see figure 3.3) will change depending on the distance to the target  $d$ , and the sun angle. Since this is the surface for which slope error is calculated, slope error will change depending on these values. Slope error will also change depending on the relative rotation of the mirror panel, as the mirror panel's principal RoCs might line up better with the segment of ideal paraboloid

### 3. Literature Review

at one rotation, than at another. The combination of distance  $d$ , angle with the sun and the mirror rotation that minimises the slope error, will define the best fit section of paraboloid, and hence the best position for the panel on a dish.



Figure 3.4.: Flux distribution of a mirror panel's focused spot.

In practise, these quantities are rarely altered to find the optimum. It would be a massively time consuming process to take enough measurements at different quantity combinations, to find a minimum. Also the mirror panel and target are normally both positioned on the ground, which means sun angle is purely determined by the elevation of the sun in the sky.

In practise photographs are taken at a few different target distances about the point which produces the best focus to the eye, and then the same photos are taken but with the panel rotated  $90^\circ$ . This is all performed with the sun at a relatively low elevation in the sky. This allows the panel RoCs to be approximated and slope errors to be more consistently compared to the measurements on other panels. Also the rim angle of the SG4 dish is around  $50^\circ$ , so any sun angles higher than this will be comparing the mirror panels to a surface which they will never be placed on.

For research purposes flux mapping is quite a cheap and effective method. However it is far from ideal for production scale testing of individual mirror panels, since it is slow and it can only be performed on a clear day with the sun at a low elevation.

## 3.3. Dial Gauge Measurements

Taking dial gauge measurements was the standard way of measuring mirror panel RoCs at the STG, before mirror panel photogrammetry was developed. Figure 3.5 shows a dial gauge measurement taking place. The mirror panel is supported by either 3 or 4 bolts. A digital dial gauge is suspended above the mirror on a rail. The tip of the dial gauge touches the mirror surface. It is slid along the rail, with measurements taken at set intervals. Two sweeps are taken, running  $90^\circ$  to one another, across the panel centre.

Only a limited number of points on the mirror surface are used to calculate the RoCs, so it is highly susceptible to error from local deformations. In practice these

### 3. Literature Review

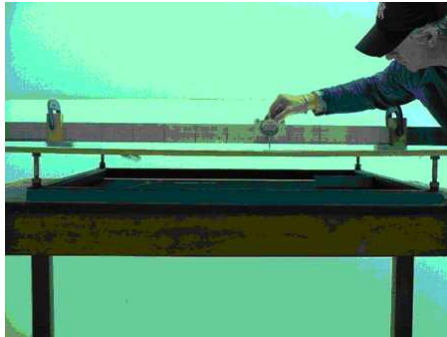


Figure 3.5.: Dial gauge measurement being performed by STG staff member.

measurements have been found to give inconsistent results with a systematic error (Burgess, G., pers. comm., Sept 2009). Also the fact that the RoCs are always measured along the mirror panel axes, means that the measured values might not be the principal RoCs.

## 3.4. Deflectometry

Deflectometry is a term that loosely encompasses measurement techniques that work by analysing how light is either reflected from a specular surface, or how it is refracted through a transparent medium. In the last few years research has gone into applying deflectometry to solar concentrators.

Kammel & Puente León (2005) describe a deflectometry system in their paper titled *Deflectometric Measurement of Specular Surfaces*. This system was developed as a quality control method for detecting visually unpleasing defects in specular surfaces. Such applications include car bodies, windshields, dies and moulds. For these needs, the deflectometric method is said to outperform conventional triangulation methods.

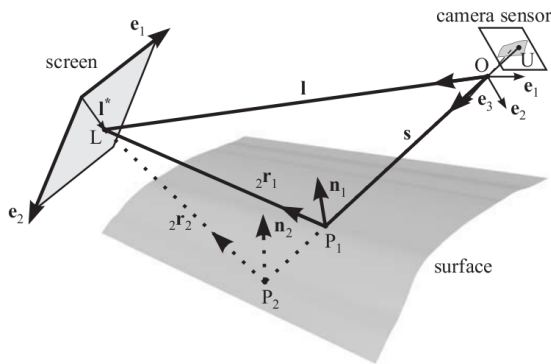


Figure 3.6.: Proposed deflectometry setup (Kammel & Puente León 2005). Intensity pattern on screen reflects off the surface to be measured into camera lens.

### 3. Literature Review

The method works by taking a photograph of the reflection of an intensity pattern in a specular surface (see figure 3.6). The distortion of the screen intensity pattern in the mirror, allows the local surface curvature to be calculated.

A reference surface is required in order to calculate these curvatures. This approach is seen as being a problem in many cases, as reference data is not always available. It uses phase shifting techniques to determine the source point of light on the screen, which requires multiple photos to be taken of different intensity pattern phases. A measurement taken of a car door can be seen in figure 3.7.

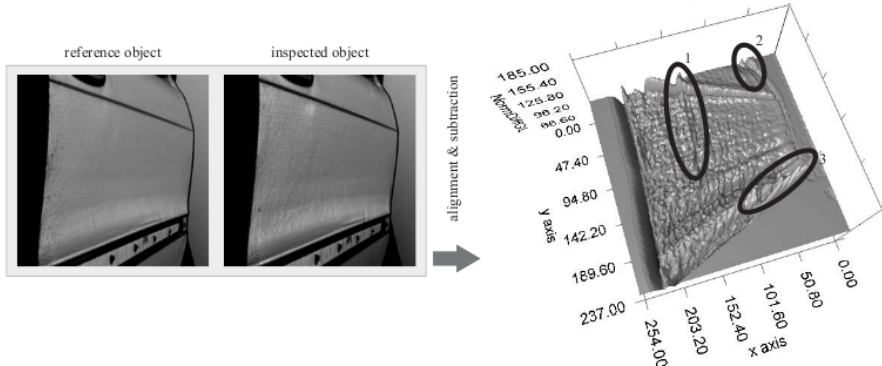


Figure 3.7.: Measurement taken of car door showing defects (Kammel & Puente León 2005).

The Ondulo system developed by EOS Technologies Inc. uses a similar deflectometry method for checking the quality of painted car bodies. The primary purpose of this system is to determine the local curvatures of the surface (Fernholz et al. 2007). Tight surfaces curvatures typically correspond to unsightly defects.

EOS Technologies Inc. have also developed a deflectometry system for measuring the slope errors of heliostat facets, as described in their brochure *QualiSURF-R: Solar Applications*. They give a brief description of a system that could be used to measure the slope error of mirror facets and parabolic troughs. A periodic grid pattern is reflected in the mirror surface in a test enclosure as shown in figure 3.8. A camera captures the reflection and “QualiSurf-R is able to quantify the local mirror slope and consecutive ray target error”. Surface slopes are calculated to better than  $15 \times 10^{-3} \mu\text{m}/\text{mm}$  ( $\sim 0.015 \text{ mrad}$ ).

This is a method that only surfaced recently. It promises to provide quick and highly accurate slope error measurements, but it doesn't mention anything about measuring surface positions and hence mirror panel RoCs. For a heliostat with flat panels this might not be a problem, but it is an important requirement for quantifying the surface of mirror panels for a parabolic dish.

*Slope Measurements of Parabolic Dish Concentrators Using Color-Coded Targets* by Ulmer et al. (2008), describes an accurate method of measuring the slope errors of a whole parabolic dish. The paper describes how the setup shown in figure 3.9 works:

“This method uses a flat target with colored stripes placed close to

### 3. Literature Review



Figure 3.8.: Potential setup of QualiSURF system (from *QualiSURF-R: Solar Applications* broacher, EOS Technologies Inc.).

the focal plane of the concentrator and a digital camera located at an observation point on the optical axis at some distance from it. A specially developed image analysis algorithm detects the different colors of the images of the reflection of the target in the concentrator and assigns them their known position on the color target. This information, along with the geometry of the measurement setup and the theoretical parabolic shape of the concentrator, is used to calculate the normal vectors of the concentrator surface. From these normal vectors, the radial and tangential slopes can be calculated and compared to the design values of the concentrator.”

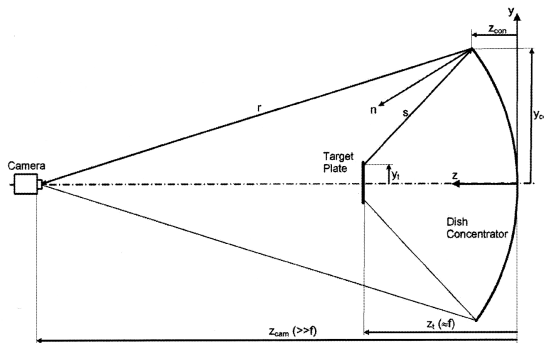


Figure 3.9.: Setup of color-coded dish measurement system (Ulmer et al. 2008).

The paper describes how the resulting measured surface was ray-traced, and how this flux distribution was compared to actual flux measurements. The two methods were found to agree well with each other.

A technique similar to this but applied to parabolic troughs instead of dishes is described in *Slope Error Measurements of Parabolic Troughs Using the Reflected Image of the Absorber Tube* by Ulmer et al. (2009). This technique known as the “absorber reflection method” uses the trough absorber tube itself instead of

### *3. Literature Review*

a color-coded target, and a series of photographs need to be taken at slightly different trough tilt angles. The slope errors obtained using this method were found to agree well with those from measurements made with photogrammetry.

These last two methods are quite effective at measuring slope error, however they don't give information on RoCs, so would have limited use applied to mirror panels. They also require the camera to be placed a long distance from the concentrator, which would take up a lot of space in a laboratory or manufacturing plant.

## 4. Coloured Pattern Deflectometry

This chapter describes the theory behind a new deflectometry method named Coloured Pattern Deflectometry (CPD). CPD measures the surface positions and normals of a mirror panel, which allow both RoCs and slope errors to be calculated, as described in chapter 2. This method was designed to best meet the measurement requirements of a mirror panel, at a low cost and with ease of use and simplicity in mind.

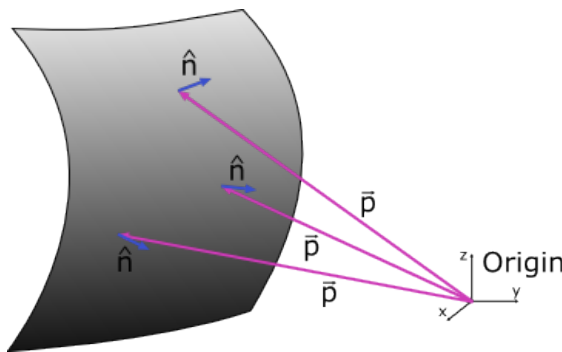


Figure 4.1.: Position vectors (pink) and surface normals (blue) for 3 points on a surface.

The method was designed by gathering ideas from existing methods, and coming up with unique solutions for the specific requirements. These design decisions will be explained throughout the chapter.

This chapter starts off with an overview of the method and how surface positions and normals are calculated. It then breaks down into sections that explain in more depth important parts of the process. The final part of the chapter looks at a simulation that was run to test the performance of the method.

The following notion is used to representing vectors:

$\vec{v}$  vector

$\hat{v}$  unit vector

$v$  vector magnitude

$v_x$  vector x component

#### 4. Coloured Pattern Deflectometry

## 4.1. Overview

The basic setup of the CPD method is shown in figure 4.2. A camera views the reflection of a patterned object in the surface of a mirror panel. A photograph is taken and the resulting image is processed. For each pixel that views a section of the mirror, a mirror surface position and normal vector are calculated. Figure 4.2 shows the path of one light ray, traced from its starting point on the pattern, to its destination a camera pixel.

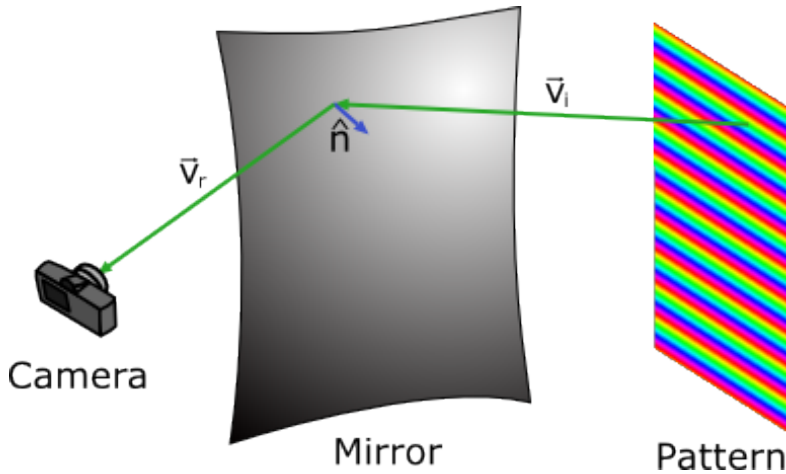


Figure 4.2.: Basic measurement setup. The path of a light ray originating on the pattern surface is shown, as it reflects off the mirror into the camera.

Given the incident and reflected light ray unit vectors ( $\hat{v}_i$  and  $\hat{v}_r$ ), the surface normal of the mirror is given by (vector form of law of specular reflection):

$$\hat{n} = \frac{\hat{v}_r - \hat{v}_i}{|\hat{v}_r - \hat{v}_i|} \quad (4.1)$$

The reflected unit vector can be determined for a given image pixel if the orientation of the camera is known (see section 4.2). However in order to calculate the incident vector, the point where the light ray leaves the pattern  $\vec{p}_{pat}$  must be known, as well as the point where it strikes the mirror surface  $\vec{p}_{mir}$ :

$$\vec{v}_i = \vec{p}_{mir} - \vec{p}_{pat} \quad (4.2)$$

$$\hat{v}_i = \frac{\vec{v}_i}{v_i} \quad (4.3)$$

$\vec{p}_{pat}$  can be worked out from the colour of the pixel (see section 4.3). However the mirror surface position  $\vec{p}_{mir}$  is the other unknown we are trying to measure. This leaves a bit of a problem, since it appears that the mirror surface normal can not be determined without first knowing the mirror surface position and vice versa. An illustration of this problem is given in figure 4.3. Here the same source point is

#### 4. Coloured Pattern Deflectometry

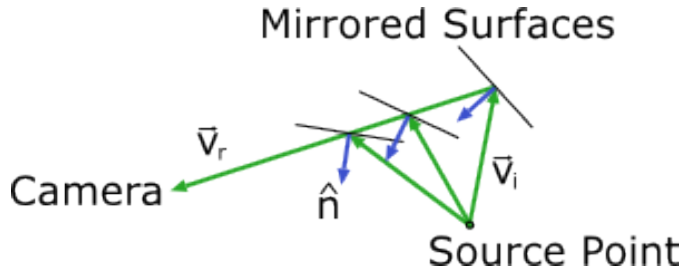


Figure 4.3.: Different mirrored surfaces can reflect the same pattern source point into the same camera pixel. This means that there is an infinite number of mirror surfaces which could produce identical results in camera.

reflected into the same pixel in the camera, but different mirrored segments cause the reflections.

The approach taken to get around this, is to anticipate the rough position of one point on the mirror surface. The surface normal can then be calculated for the point. This information can then be used to find the surface position of a neighbouring point by extrapolating the surface out (see section 4.4).

The following sections will explain in more depth how the reflected light vector, pattern source point and surface positions are calculated.

## 4.2. Reflected Light Vector

A directional vector can be assigned to each pixel in the camera sensor. This vector defines where light absorbed by the pixel originated from, and can be used to determine the reflected light ray vector  $\hat{v}_r$  for a pixel.

Figure 4.4 shows how an object point is focused onto the sensor array within a digital camera. Here the thin lens approximation has been used where all principal and nodal points are assumed to coincide at the centre of the lens (see appendix B for further details on lens optics). All 3 light rays in the figure enter the camera from different directions, even though they originate from the same point in focus. The light ray that traverses the nodal points of the lens, (the centre of the lens in this case) is taken to be the direction from the camera to the point in focus, for a given pixel.

The local coordinates for the camera are marked at the origin of the lens in figure 4.4. The x axis protrudes out of the page. The direction to a point in focus can be worked out from its vector components. A ray that traverses the nodal points will be parallel to itself, as it enters and leaves the lens. Therefore we can just work out the vector direction on the imaging side of the lens. The z component of this directional vector will simply be equal to the principal distance. The x and y components will depend on the distance between the pixel, and where the optical axis strikes the sensor array. Ideally the optical axis would pass through the centre of the sensor array, however in practice it tends not to. In photogrammetry this point is often called the principal point, which is different for the principal point

#### 4. Coloured Pattern Deflectometry

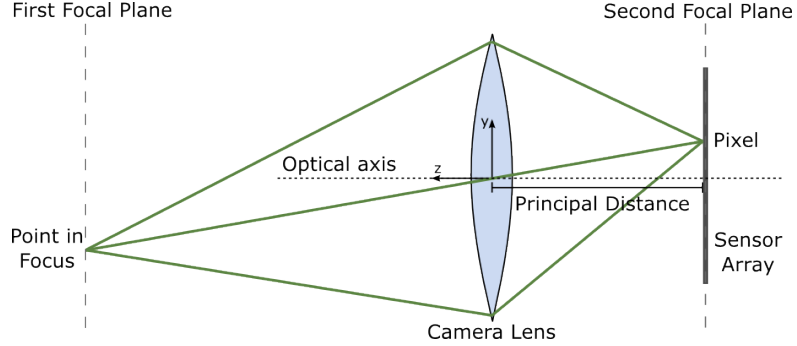


Figure 4.4.: The lens and sensor array of a digital camera. Shown are 3 of the many paths light can travel from a point in focus, to its corresponding pixel in the camera array. The principal distance is the distance along the optical axis from the principal point to the sensor array.

used in optics (which is at the opposite end of the principal distance). To avoid confusion we will instead call it the sensor optical centre. The x component of the vector direction is:

$$v_x = (pix_x - w_x/2 + 0.5) \cdot pxsizex - soptcx \quad (4.4)$$

Here  $w_x$  is the pixel width of the sensor array along the x direction,  $pix_x$  is the pixel number between 0 and  $wid_x - 1$ ,  $pxsize$  is the physical width of one pixel, and  $soptcx$  is the physical position of the sensor optical centre relative to the centre of the sensor array. The y component can be calculated in the same way.

The direction of the reflected light ray is now known in terms of the camera coordinate system. However this information is required in terms of a global coordinate system, in order to work with other parts of the system. To convert between these two systems, the position and orientation of the camera needs to be known in terms of global coordinates.

The camera could be fixed at a given location and orientation, so that it would only need to be measured once. However a more adaptable approach was taken where the camera location can be computed by information stored in the measurement photographs themselves.

The idea is that 3 reference dots are arranged around the mirrored surface, which define the x-y plane of the global coordinate system. These dots are positioned so that they are captured in a measurement photograph. This idea was adapted from a similar idea used by the STG to locate the camera for flux maps. Figure 4.5 shows the arrangement of the dots about the mirror panel.

The directional vectors  $\hat{v}_1$ ,  $\hat{v}_2$  and  $\hat{v}_3$  are calculated in terms of camera coordinates, by using the method described at the beginning of this section. The corresponding magnitudes of these vectors are the unknowns  $v_1$ ,  $v_2$  and  $v_3$ . The distance  $d$  between each dot is known. The relation is then given by:

$$d_{12} = |\vec{v}_2 - \vec{v}_1| \quad (4.5)$$

#### 4. Coloured Pattern Deflectometry

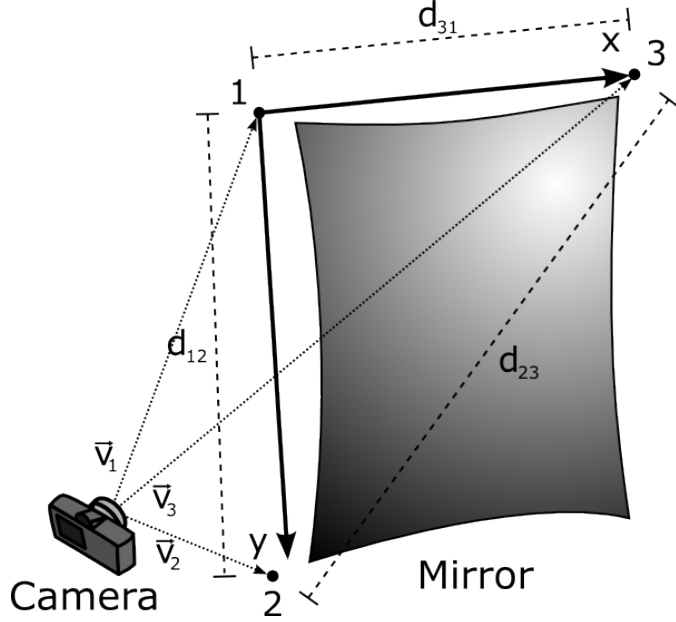


Figure 4.5.: Global coordinates and 3 reference dots positioned around mirror.  
Note that dot 2 does not necessarily lie along the y axis, but it is in x-y plane.

$$\Rightarrow d_{12}^2 = (\vec{v}_2 - \vec{v}_1) \cdot (\vec{v}_2 - \vec{v}_1) \quad (4.6)$$

$$= \vec{v}_2 \cdot \vec{v}_2 - 2\vec{v}_2 \cdot \vec{v}_1 + \vec{v}_1 \cdot \vec{v}_1 \quad (4.7)$$

$$= v_2^2 - 2v_2 v_1 \hat{v}_2 \cdot \hat{v}_1 + v_1^2 \quad (4.8)$$

For the other two distances:

$$d_{23}^2 = v_3^2 - 2v_3 v_2 \hat{v}_3 \cdot \hat{v}_2 + v_2^2 \quad (4.9)$$

$$d_{31}^2 = v_1^2 - 2v_1 v_3 \hat{v}_1 \cdot \hat{v}_3 + v_3^2 \quad (4.10)$$

This is a system of 3 non-linear equations with 3 unknowns  $v_1$ ,  $v_2$  and  $v_3$ . This can be solved by numerical means.

Each of the 3 global coordinate vectors need to be calculated in terms of the camera coordinates in order to construct the transformation matrix between the two systems. The 3 global coordinates are given by the equations:

$$\hat{g}x = \frac{\vec{v}_3 - \vec{v}_1}{|\vec{v}_3 - \vec{v}_1|} \quad (4.11)$$

$$\hat{g}z = \hat{g}x \times (\vec{v}_2 - \vec{v}_1) \quad (4.12)$$

$$\therefore \hat{g}z = \frac{\vec{g}z}{|\vec{g}z|} \quad (4.13)$$

$$\hat{g}y = \hat{g}z \times \hat{g}x \quad (4.14)$$

#### 4. Coloured Pattern Deflectometry

Where  $\hat{g}x$ ,  $\hat{g}y$  and  $\hat{g}z$  are the global coordinates in terms of camera coordinates. The transformation matrix is built from these vectors:

$$\mathbf{T} = \begin{pmatrix} gx_x & gx_y & gx_z \\ gy_x & gy_y & gy_z \\ gz_x & gz_y & gz_z \end{pmatrix} \quad (4.15)$$

A directional vector can be transformed between the two coordinate systems by:

$$\vec{v}_{gc} = \mathbf{T}\vec{v}_{cc} \quad (4.16)$$

A position vector is transformed by:

$$\vec{v}_{gc} = \mathbf{T}(\vec{v}_{cc} - \vec{v}_1) \quad (4.17)$$

These transformations allow the reflected vector, calculated in terms of camera coordinates, to be transformed to the global coordinate system.

### 4.3. Pattern Source Position

The coloured pattern provides a way of working out the source position of the reflected light ray. There are many different types of patterned surfaces that could be used for this purpose. The initial idea to use colour in the pattern, came from reading the color-coded target paper by (Ulmer et al. 2008). The actual design of the pattern however, needed to be quite different, so that high resolution slope measurements could be made over short distances.

The coloured gradient acts as a ruler, where the hue value of light leaving the surface can be converted to a distance. Using a coloured pattern has lower costs than phase-shifting techniques, which require a screen (such as a monitor or projector) that can change a pattern. It also has an increased robustness over a simple luminosity gradient.

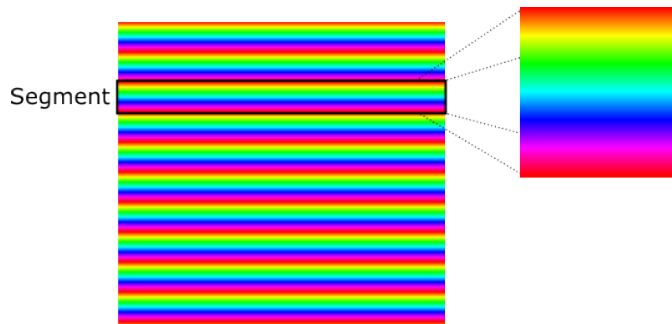


Figure 4.6.: Target pattern colour gradient.

The pattern is broken up into repeating segments as shown in figure 4.6. The hue values change continuously in one segment, returning to the same hue that the

#### 4. Coloured Pattern Deflectometry

segment starts on. If a light ray of a given green hue is absorbed by a camera pixel, then the light ray must have originated from a point along one of the lines marked on figure 4.7. If the patterned surface is then rotated 90° and another observation made, the reflected hue value will be different (say orange). Figure 4.8 shows a line of points where this orange hue must have originated from. Superimposing these two measurements, the possible source locations have now been limited to the points shown in figure 4.9.

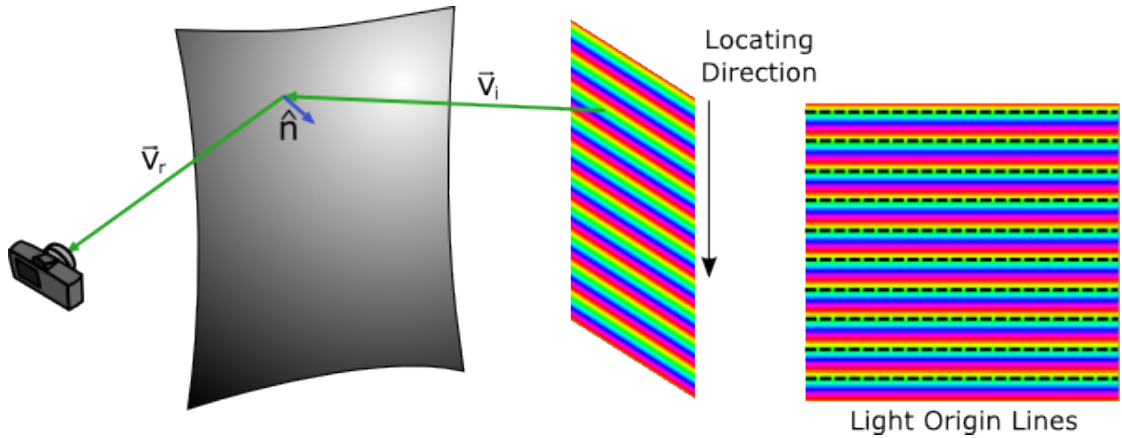


Figure 4.7.: Measurement setup with a horizontally aligned pattern. A perpendicular view of the pattern is given showing lines of potential source points for a green light ray.

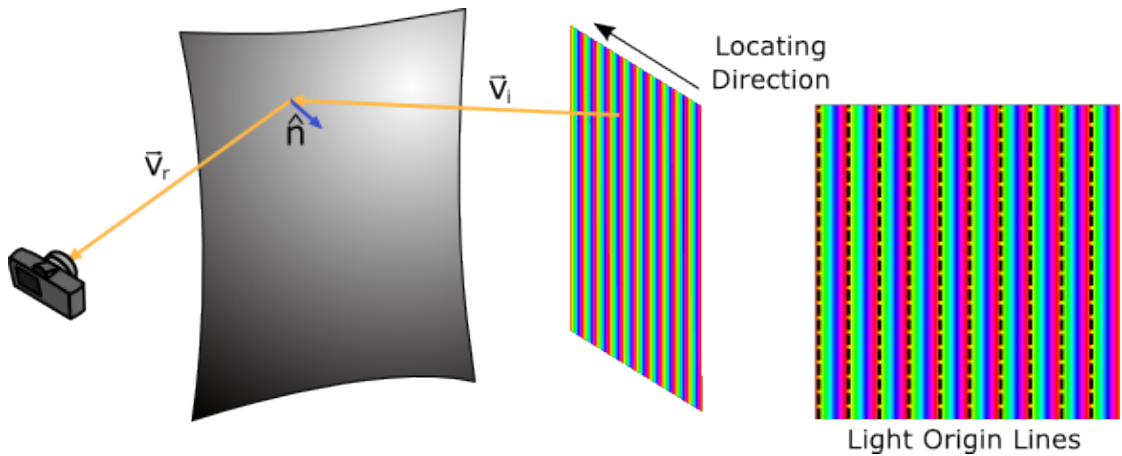


Figure 4.8.: Measurement setup with a vertically aligned pattern. A perpendicular view of the pattern is given showing lines of potential source points for an orange light ray.

If the patterned surface had been made up of only one large segment, there would only be one potential source point at this stage. However for most applications a camera will not have enough resolution in hue to give a high enough spacial

#### 4. Coloured Pattern Deflectometry

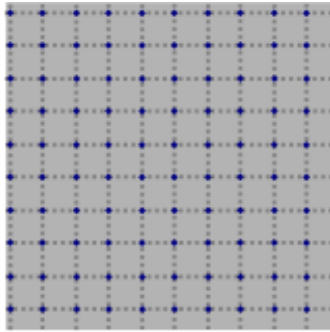


Figure 4.9.: Silhouette of pattern with source lines superimposed. Potential source points are given by blue dots.

resolution on the pattern, with only one segment. Therefore the problem remains of determining which of these points the light ray originated from.

This can be done by working out the starting segment for one pixel in the camera, and by assuming a certain smoothness of the mirror. For example, say that one pixel in the camera is known to receive a light ray from the top right corner of the pattern (within the top segment of the horizontally aligned pattern, and the right most segment of the vertically aligned pattern). If this light ray was green and orange for horizontally and vertically aligned patterns respectively, then the source point must be the top right most point identified in figure 4.9. If the mirrored surface is smooth then the source location of a neighbouring pixel must not be far from the source point of this pixel. If the mirror is sufficiently smooth then two neighbouring pixels will not have source locations further than half a segment apart. Using this rule and calculating pixel source positions one at a time, working away from the starting pixel, the whole mirrored surface can have its light source positions calculated.

The smaller the segment size, the higher the pattern surface position resolution since the colours are spaced over a smaller distance. This will increase mirror surface resolution. However if a segment is too small, then there is a greater risk that two neighbouring camera pixels reflect a part of the pattern that is more than half a segment apart. This could lead to misidentification of a pattern source point.

The size of a pattern segment should be chosen by considering the distance to the mirror panel, and the smoothness of the mirror surface. Figure 4.10 shows how the minimum segment size can be calculated. Point 1 and 2 on the pattern surface correspond to neighbouring pixels in the camera. Both mirrored surface reflection points have been superimposed since they are close to one another, and the reflection vector  $\vec{v}_r$  is assumed to be the same for neighbouring pixels. The coloured pattern is assumed to be  $\sim 90^\circ$  to the incident vectors, and at a distance of  $d_{patt}$ .  $\theta_{max}$  is the maximum expected change in surface slope, for two neighbouring pixels, which is an indication of the surface smoothness. The segment width should therefore be no less than:

#### 4. Coloured Pattern Deflectometry

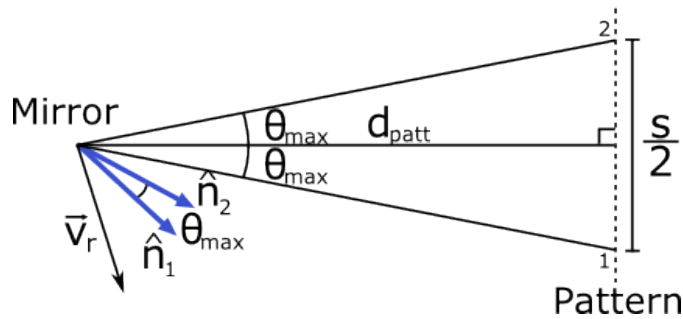


Figure 4.10.: Reflection of two points on pattern surface into neighbouring camera pixels.

$$s = 4d_{patt} \tan \theta_{max} \approx 4d_{patt}\theta_{max} \quad (4.18)$$

In practice there is not a continuous range of hue values in a segment. There must be some resolution, either due to screen pixel size or printer resolution or to the maximum number of hues the camera can distinguish. Figure 4.10 can be used to work out how this translates to a surface slope resolution. In the figure assume that  $s/2$  is now equal to the smallest distance that can be represented on the pattern surface  $s_{res}$ . This could for example be limited by the resolution of the printer used to print the pattern. Replace  $\theta_{max}$  with the slope resolution  $\theta_{res}$ , and equation 4.18 becomes:

$$\tan \theta_{res} \approx \theta_{res} = \frac{s_{res}/2}{d_{patt}} \quad (4.19)$$

The plane in which the pattern lies and its position must be known in order to calculate the pattern source locations in terms of global coordinates.

## 4.4. Surface Position

Other deflectometry systems don't calculate surface positions, instead they use either a reference or ideal surface to calculate surface slopes. However they are required in order to calculate mirror panel RoCs.

The approach taken calculates surface positions in an iterative manner, similar to how the pattern source positions are calculated. A surface position is assumed for a starting pixel and its surface normal is calculated. If the mirrored surface is sufficiently smooth then the slope of the surface won't change much between one pixel and its neighbour. This allows the surface position of a neighbouring pixel to be estimated by extrapolating the surface out to intercept the reflected vector of the neighbour pixel. The slope of this neighbouring pixel is then calculated and the process continues.

Figure 4.11 shows the vectors relating two surface points for neighbouring pixels. The surface position and normal is known for the first pixel. Assuming the second

#### 4. Coloured Pattern Deflectometry

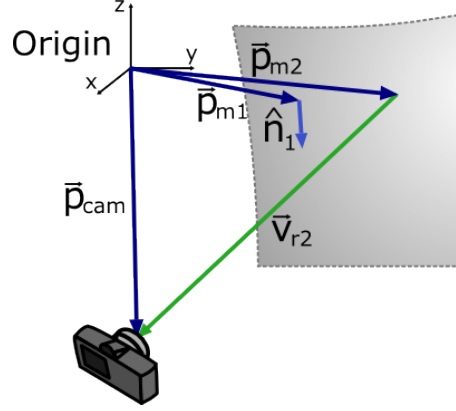


Figure 4.11.: Two surface points corresponding to two neighbouring pixels in the camera. The surface position and slope of the first point is known.

surface point is positioned perpendicular to the surface normal of the first surface point, then:

$$(\vec{p}_{m2} - \vec{p}_{m1}) \cdot \hat{n}_1 = 0 \quad (4.20)$$

$$\Rightarrow \vec{p}_{m2} \cdot \hat{n}_1 - \vec{p}_{m1} \cdot \hat{n}_1 = 0 \quad (4.21)$$

$$\Rightarrow \vec{p}_{cam} \cdot \hat{n}_1 - v_{r2} \hat{v}_{r2} \cdot \hat{n}_1 - \vec{p}_{m1} \cdot \hat{n}_1 = 0 \quad (4.22)$$

$$\Rightarrow v_{r2} = \frac{(\vec{p}_{cam} - \vec{p}_{m1}) \cdot \hat{n}_1}{\hat{v}_{r2} \cdot \hat{n}_1} \quad (4.23)$$

The relation  $\vec{p}_{m2} = \vec{p}_{cam} - v_{r2} \hat{v}_{r2}$  has been used to get equation 4.22, and can be used to work out the surface position of the second point.

This approach requires the position of one starting point on the mirror surface to be known. The idea is to roughly position a mirror panel so that the position of a starting point on the mirror surface is roughly known. It is difficult to calculate what the effects will be of not knowing the exact position of the starting point. This was the main motivation for performing the simulation in the next section.

## 4.5. Simulation

A python script named *interrors.py* was written to model the deflectometry method. This simple model provides a quick way to get a indication of the expected errors, and for determining which conditions give the best results. The model comprises of the setup shown in figure 4.12.

The model works on a 1D curve instead of 2D surface. It assumes that the reflected vector and pattern source position can be calculated without error. A circular curve is built to act as the test surface. The model starts solving positions and slopes at one end of the curve. The starting point is offset from the curve by  $h_{err}$ , to simulate an error in positioning the mirror panel. For a given camera it

#### 4. Coloured Pattern Deflectometry

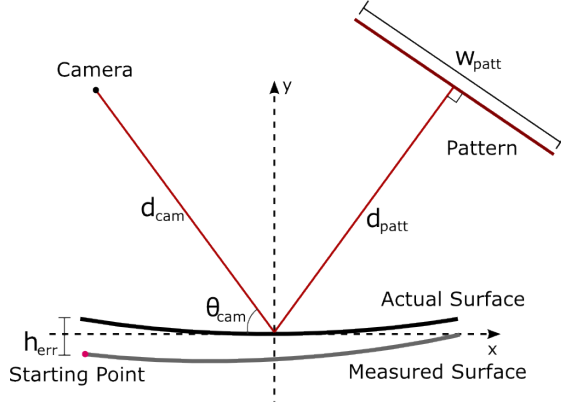


Figure 4.12.: Model setup.

calculates for each pixel the resulting source location on the pattern. It then uses this data to work out the measured position of the surface. Surface slopes can then be calculated.

Once the surface has been built, a circle is fit to the data. The RoC of the fitted circle can then be compared to the original curve, and slope errors can be calculated.

A series of tests were run on a 30m RoC circle test curve. The results are given in table 4.1.

Table 4.1.: Simulation results.

$d_{cam}$ (m)	$\theta_{cam}$ ( $^{\circ}$ )	$d_{patt}$ (m)	$h_{err}$ (mm)	$\Delta R$ (%)	$\varepsilon_{max}$ (mrad)	$w_{patt}$ (m)
4.0	60	2.0	1	-0.20	0.022	1.41
3.0	60	2.0	1	-0.26	0.019	1.59
3.0	60	2.0	2	-0.52	0.021	1.59
1.5	60	2.0	1	-0.49	0.036	2.25
3.0	60	3.0	1	-0.17	0.018	1.85
2.5	60	2.0	1	-0.33	0.017	1.73
2.5	75	2.0	1	-0.43	0.016	1.93
2.5	60	2.5	1	-0.26	0.016	1.90
2.5	90	2.0	1	-0.49	0.026	1.99

$\Delta R$  is the percent change in the measured RoC from the actual. The max slope error gives an indication of how the slope error of a panel will be effected by using this deflectometry method.

The following trends were found from the simulation results:

- Increasing camera distance produces a better matching curve and smaller required pattern width. However this is true only to a limit that depends on

#### 4. Coloured Pattern Deflectometry

the focal length of the camera used. As the camera becomes further away, fewer pixels capture the surface, so the surface resolution is lowered. This can produce poor fitting results and potentially miss fine details.

- A more acute viewing angle produces a slightly better matching curve but again as the angle gets too sharp, surface resolution is lost in one of the dimensions.
- A more distant pattern produces a better matching curve, but it increases the required pattern size.
- As expected, having a larger initial offset error produces poorer matching results.

The errors between the measured and fitted curves were calculated and plotted in figure 4.13 for the first five configurations in table 4.1. The slope errors for these 5 configurations are given in figure 4.14.

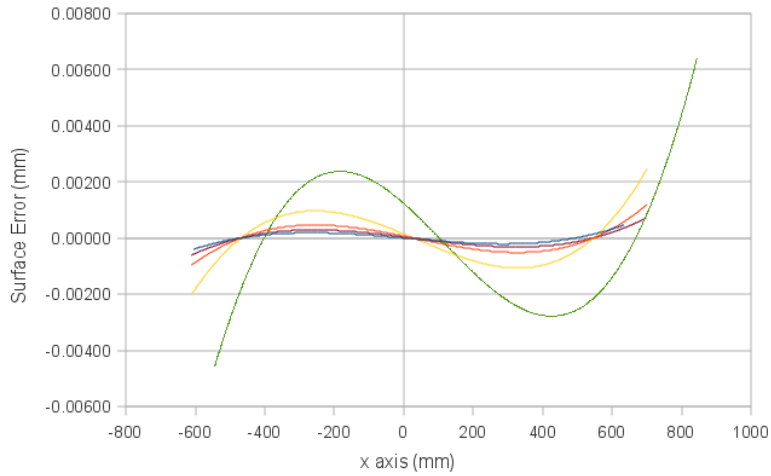


Figure 4.13.: Error between measured surface and fitted curve.

All five of these configurations produce curves that are within  $5\mu\text{m}$  of the fitted curves. This explains why the slope errors are so small.

These simulation results show that the method in principal should produce accurate results as applied to a 1D curve. This assertion can not be simply extended to the realm of a 2D surfaces. Figure 4.15 shows the difference between the measured curve and actual curve for the second configuration in table 4.1. The measured shape converges towards the actual curve as it is solved. Between the start and the end the gap changes by around  $300\mu\text{m}$ . This does not effect the fitted RoC since the overall shape of the measured surface is preserved, it has just been rotated towards the actual surface.

If the starting point was located at the other end of the curve then the measured surface would diverge away from the actual surface. Whether or not the surface

#### 4. Coloured Pattern Deflectometry

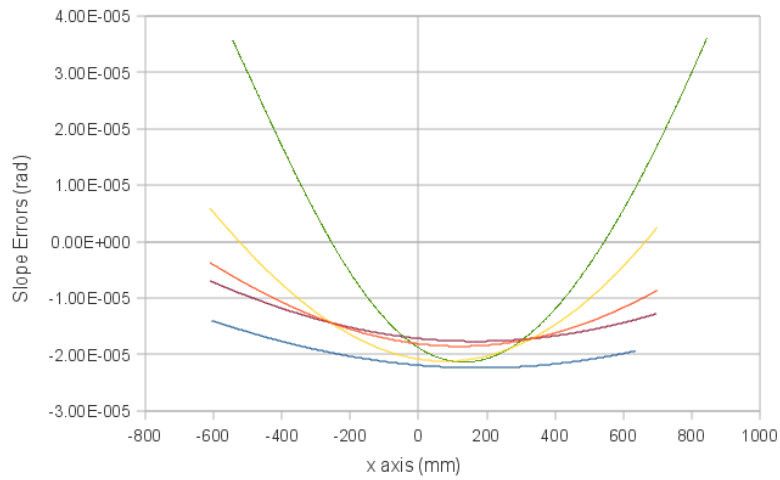


Figure 4.14.: Slope errors calculated relative to fitted surface.

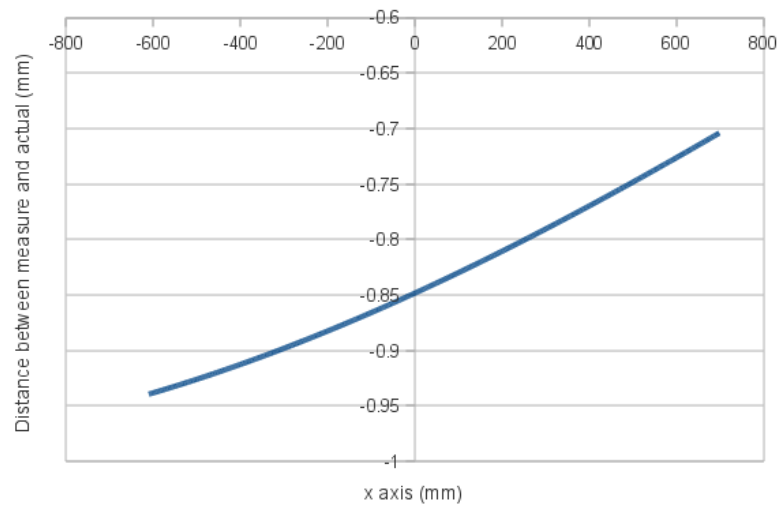


Figure 4.15.: Difference between measured curve and actual curve, for the second set of parameters in table 4.1.

#### *4. Coloured Pattern Deflectometry*

diverges or converges depends on whether or not the solution path progresses in the same direction as the camera points, or against it. Whereas for a 1D curve all this results in is a rotated surface, for a 2D surface it could end up producing a warped surface.

# 5. Implementation

An implementation of the CPD method, was designed and built. This chapter describes the design choices, construction, and programming that took place. The components include a frame to hold the mirror panels, the coloured pattern and its supporting frame, and image processing and analysis software.

## 5.1. Construction and Calibration

Figure 5.1 shows the layout of the finished deflectometry setup. Considering the space limitations of the workshop, the requirement for a compact system, and the simulation results in section 4.5, a layout with  $d_{cam} = 3\text{m}$ ,  $d_{patt} = 2\text{m}$  and  $\theta_{cam} = 60^\circ$  was selected. The following sections contain descriptions of the mirror panel frame, and the coloured pattern frame.



Figure 5.1.: Deflectometry setup. Mirror frame is on the left and the coloured pattern on the right.

### 5.1.1. Mirror Frame

The mirror frame holds a mirror panel in place as it is measured. It was designed so that a mirror panel rests vertically as it is being measured, because gravity has a significant affect on a panel's RoC while supported horizontally. The frame also includes the 3 reference points used to locate the camera and a disk locator for lining up the top left edge of a mirror panel.

The frame was designed to bolt onto the top of a workshop bench. A mirror panel is placed on the feet of the frame, and held at the top by a spring loaded

## 5. Implementation

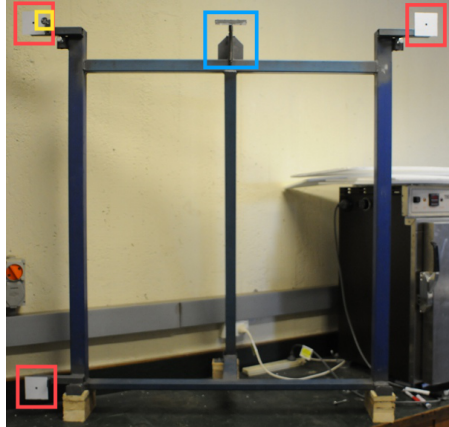


Figure 5.2.: Frame for holding mirror panel. Red highlights the 3 reference dots, yellow the mirror locating disk and blue the panel clamp.

clamp. The bolts at the top corners give the panel something to rest against. The metal disk protruding from the top left corner of the frame acts as a guide for lining up the top left corner section of mirror (see figure 5.3). The position of this disk is fixed so that the deflectometry software has a known starting surface depth.



Figure 5.3.: Close up of the locating disk. The plane of the top left corner of the mirror panel is lined up with the plane of the locating disc.

The technique of photogrammetry (described in section 3.1), was used to accurately measure the relative locations of the 3 reference dots and the locating disk. Six dots were positioned on the frame uprights to act as photogrammetry references. As a requirement for the photogrammetry, the relative positions of these points were measured to within a few millimetres with a tape measure. Additional dots made on a laser printer, were placed around the frame, to allow for a better photogrammetry solution.

Around 20 photographs were taken of the frame and surrounding dots from varying angles. The same basic approach was taken to process the images, as Burgess et al. (2009) use for mirror panels. The differences were that printed instead of projected dots were used, and simple reference dots instead of coded

## 5. Implementation

targets were used. The resulting dot locations were positioned with a mean error of around  $30\mu\text{m}$ .

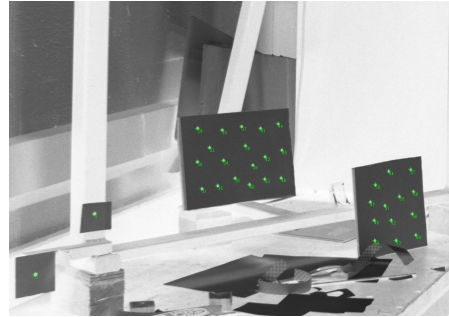


Figure 5.4.: One of the photogrammetry images for the mirror frame.

### 5.1.2. Coloured Pattern

The coloured pattern was printed onto two sheets of paper that when combined make a  $2\text{m} \times 2\text{m}$  square. The pattern is glued to a sheet of MDF to give it some rigidity and keep it flat. This MDF has a backing support with a rod that sticks out from its centre. This rod sits in two bearings that allows the whole MDF sheet and pattern to rotate about its centre. The whole thing is supported by a frame that extends to the floor, where it is bolted to the concrete.



Figure 5.5.: Back of coloured pattern showing frame. The blue area highlights the bearings and shaft holding coloured pattern. Orange highlights the locking pin used to hold the pattern in place.

The size of the pattern was selected to be a little larger than the size suggested by the simulation performed in section 4.5. The pattern is made of 42 repeating segments. Each segment is made from a gradient of 135 different colours. These

## 5. Implementation

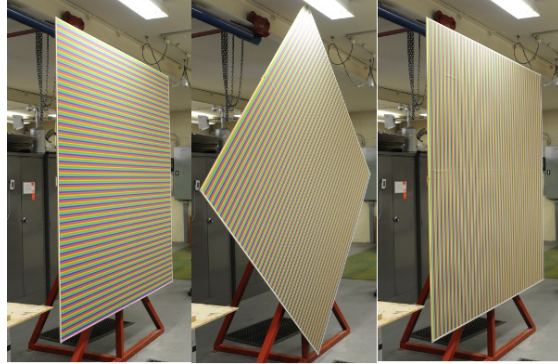


Figure 5.6.: Coloured pattern being rotated.

colours were picked from the HSL colour space. The colours transition linearly through the range of available hues ( $H = 0.0 \rightarrow 1.0$ ), while holding the saturation and level values constant ( $S = 1.0$ ,  $L = 0.5$ ). A section of the printed pattern can be seen in 5.7.

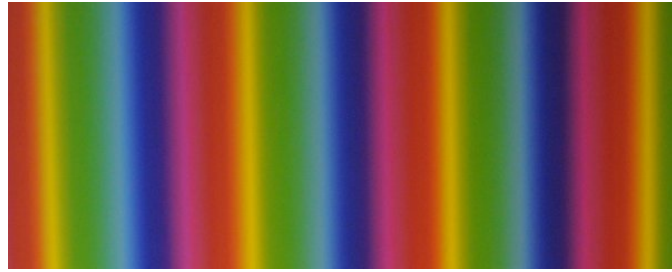


Figure 5.7.: Up close photograph of printed colour pattern. A segment transitions from red at  $H = 0.0$ , through yellow, green, blue, purple and then back to red at  $H = 1.0$ .

The pattern was printed from a TIFF image which was created from the Python script *makepattern1d.py*. Each segment is 47.7mm wide. This segment size was selected based on the minimum segment size equation (equation 4.18). Initially a  $\theta_{max}$  value of 8mrad was selected by considering existing slope error data for mirror panels. Unfortunately a calculation error caused the pattern segment size to be underestimated (47.7mm instead of 64mm), which was not realised until after being printed. The printed segment size allows for a maximum change in surface slope of 6mrad for neighbouring pixels. While not the original intended 8mrad, it was considered good enough for all mirror panels that were intended to be measured.

The coloured pattern needed to be calibrated once it was printed. The printer, ambient lighting of the workshop, camera and camera settings, all affect how the measured hue values differ from those present in the original TIFF. First of all an experiment was conducted to determine the camera white balance setting that best represents the workshop lighting conditions. The camera used was a Nikon

## 5. Implementation

D300 with AF Nikkor 20mm 1:2.8 D lens.

Close up, square on photographs were taken of the printed pattern in the workshop lighting (shown in figure 5.7), while adjusting white balance settings for the camera. Cross sections of segments in the resulting images were taken, and the hue value of each pixel was extracted. These hue values were plotted against the pixel's position within a segment. The segment cross sections were taken at different parts of the image where the illumination varied. For example some areas of the image were bright, while shadows fell over other areas. The consistency of the segment plots under different illumination conditions, indicates how well the white balance setting matches the local environment. The cool-white fluorescent white balance setting was found to be the most reliable (see figure 5.8).

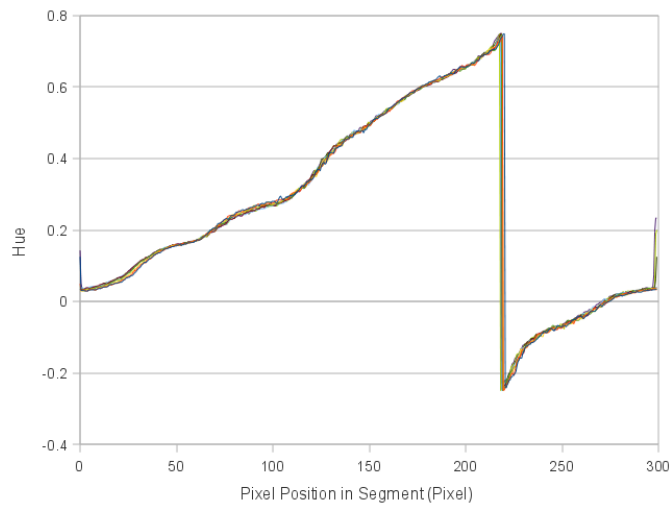


Figure 5.8.: Pixel hue plotted against pixel position within segment, for cool-white fluorescent camera setting. Curves are shown at different segment illuminations. The overlap of the curves indicates a good level of reproducibility.

One of the cool-white fluorescent segment cross sections was selected to create the calibration file for the coloured pattern. First box car averaging was applied to smooth data. It was then fed into the C program *interpatt.c*, which outputs a calibration file containing 274 values. The first entry is the fractional distance across the segment for a hue value of 0.0. The next is for a hue of 1/274, and so on all the way up to a hue of 273/274 for the 274<sup>th</sup> entry.

The distance between each hue on the coloured pattern 0.353mm. Using equation 4.19 this gives a surface slope resolution of 0.0825mrad. Even though only 135 colours were used to produce the pattern, 274 colours were measured in the calibration file. This is because neighbouring colours merge together to form a hue somewhere in between, due to printing, and leakage between pixels. If all 274 hues can be used, then there is the possibility for a surface slope resolution of 0.0435mrad. Typical good quality mirror panels have slope errors with a standard

## 5. Implementation

deviation of 1mrad.

Photogrammetry was used to measure the positions of the coloured pattern corners. Some of the dots that were measured in the mirror frame photogrammetry were measured again, so that the coordinates of the two sets of photogrammetry could be linked. This allows the position of the pattern corners to be calculated in terms of the global coordinates of the mirror frame. The pattern corners were measured a second time, but with the pattern rotated 90°. Photogrammetry solved the positions of each dot to within a mean error of 36 $\mu$ m

The Scilab script *transform.sce* was used to link the coordinates of all three sets of photogrammetry, and to then work out the transformation matrix between the coloured pattern coordinate system, and global coordinate system.

### 5.1.3. Camera Calibration

The Nikon D300 camera had previously been calibrated for its use with photogrammetry. This allowed the sensor optical centre (called principal point in photogrammetry), pixel size, principal length and radial distortion terms to be reused.

One problem was found with the camera, in that neighbouring vertical pixels would be paired together when saving an image as a TIFF. These paired pixels would have very similar, if not identical hue values. This was most noticeable when taking a picture of the coloured pattern with the segments running vertically (figure 5.9). This effect was not present in Nikon RAW images that were later converted to TIFFs. Therefore it is thought to be an artefact of the internal camera processing software for TIFFs. During experimentation it was found that this pairing effect has little influence on the deflectometry results, so TIFFs were still used out of convenience (see section 7.4).

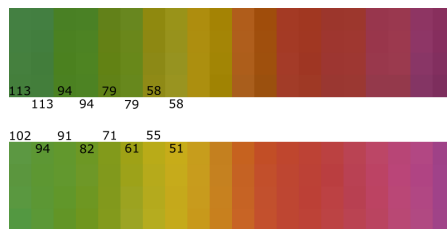


Figure 5.9.: Zoomed in section of pattern segment demonstrating vertical pairing.

The top image is a TIFF and the bottom is a RAW image. Hues are given for some pixels with values in the range of 0 → 255.

## 5.2. Programming

A program was written to process mirror panel measurement photographs, and then calculate RoCs and slope errors. The first part of this section looks at the

## 5. Implementation

program design and structure. The second part steps through the operation of the program.

### 5.2.1. Design

The Python language was originally selected for programming the deflectometry software due to its flexibility and simplicity. To assist in the design process a UML class diagram was produced. A significant portion of the program was written in Python before testing revealed that the program took 22mins to run. This long processing time would make debugging and experimenting difficult and slow. Therefore it was decided to rewrite the program in the lower level programming language C. The updated C version of the program took just 3 seconds to execute the same section of code. That is over a 400 times reduction in required processing time.

The program source code is split up into separate files. These files collect functions and parameters which are related. Each file is briefly described:

**profile.c** is the backbone of program. It contains the C *main* function, and controls the flow of the program. It includes the main mirror surface solving algorithms and data storage variables. It also performs all file I/O operations.

**camera.c** collects all functions and parameters relating to the camera. It contains camera calibration and error correction parameters. The most important functions are for locating the camera given the frame reference points, and returning the surface reflection vector for any given camera pixel.

**pattern.c** contains functions and parameters for the coloured pattern. It contains calibration parameters and a transformation matrix between the pattern coordinate system and frame coordinate system. Its functions perform operations such as extracting the hue from a pixel and returning the pattern source position for a reflected light ray.

**fitting.c** contains functions for fitting surfaces to solved mirror panel data. It can fit both a sphere and a paraboloid to mirror panel surface positions, as well as calculate surface normals for these ideal surfaces.

**commath.c** is a collection of mathematical operations which are commonly used in the above source files. It contains many matrix and vector operations, as well as a polynomial structure and conditional functions.

Figure 5.10 shows a diagram of how the different files of the program interact. A list of parameter and function names is given for each file. The program uses the GNU Scientific Library (GSL) as well as other core C libraries.

The compiled program is an executable that can be called from the command line. This executable is fed filenames for the images to process, and pixel locations

## 5. Implementation

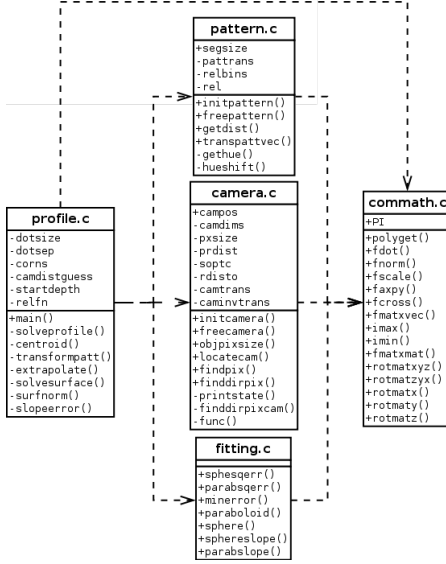


Figure 5.10.: Interaction of source files. Upper list is a file's parameters, and lower is its functions. A + indicates that the parameter/function is to be used external to the file, while a – indicates it is internal. An arrow pointing at a file indicates its functions and/or parameters are being used by file at base of arrow.

for the reference points within the image. A GUI was written in Python (version 2.6) which assists with locating the reference points, and acts as a front-end for calling the command line executable. It uses wxPython (Python binding of wxWidgets) for producing the user interface. The script is called *deflect.py*.

The program was only ever tested on a x86\_64 Linux operating system, compiled using the GNU Compiler Collection (GCC), version 4.4.1. However it should be easily portable to other operating systems (an unofficial ported version of the GSL may be required under Windows).

The final version of the program contains some 1849 lines of original code (including comments and blank lines). The GUI adds another 198 lines. It takes around 4s to perform one mirror panel calculation while running on one core of a 2.00GHz Intel processor.

### 5.2.2. Operation

Once two photographs are taken for a mirror panel (one at each pattern rotation), they can be loaded onto a computer and processed using the deflectometry software.

Once compiled the program is called from the command line using:

```
profile.o himagefn vimagefn dot1x dot1y dot2x dot2y dot3x dot3y outputfn
```

## 5. Implementation

Here `himagefn` and `vimagefn` are the horizontal and vertical image file names. The six dot parameters relate to the approximate image pixel positions of each of the three reference dots. `dot1` is the top left reference dot, `dot2` is the bottom left and `dot3` is the top right. `outputfn` is a file name to which a number results are output.

The program outputs 3 different files with the `outputfn` file name. Each of these use the comma separated value (CSV) file structure to arrange their data. The first file has the `.pos` file extension, and it includes a selection of surface position data points. The second has the `.sse` extension and it includes a selection of slope errors relative to a best fit sphere. The last file has the `.pse` extension and it also includes slope errors, but relative to a best fit paraboloid.

The program also appends a line to a file called `results.out` in the image directory. This line contains a summary of the results for the mirror panel, values such as fitted RoCs and slope error standard deviations.

When called, the program performs the following steps in order to obtain these outputs:

1. Program is run from command line passing it the file names of the two images to process, the pixel coordinates for the 3 reference points, and a file name to output data to.
2. Image with horizontally aligned pattern is loaded in from TIFF file.
3. Centroiding algorithm finds accurate centre of dots in pixels, given each dot's approximate location.
4. Camera position is calculated by solving a system of non-linear equations, using the reference dot centres.
5. Bounding area for mirrored section of picture is determined.
6. Starting at top left corner of the bounding area, the hue value of a pixel is calculated, and from this, its position within a segment is calculated. This first pixel is assumed to originate from the segment at the very top of the pattern. Subsequent pixels are calculated assuming that the segment they originate from can be no further than half a segment away from the pattern source position of neighbouring pixels. These positions are the y components of pattern source positions.
7. Delete horizontal image from memory and load in vertical image.
8. Repeat step 6 for vertical image, but this time assume that the top left pixel originates from the far right segment on the pattern. These positions are the x components of pattern source positions.
9. Transform all pattern source points from pattern coordinate system to global coordinate system of reference dots.

## *5. Implementation*

10. For top left pixel in bounding area, calculate the mirror surface normal given an assumed z depth of mirror.
11. Extrapolate out calculated surface slope to a neighbouring pixel. From this determine mirror surface position for the neighbouring pixel, and then its surface normal.
12. Repeat step 11 until all pixels in the bounding area have had their surface positions and normals calculated.
13. Fit sphere to surface positions.
14. Fit paraboloid to surface positions.
15. Calculate slope errors using surface normal data, relative to both fitted sphere and fitted paraboloid.
16. Save fitted RoC values and slope error standard deviations to `results.out`.
17. Save a selection of mirror surface positions and slope errors to disk using output file name.

# 6. Experimental Methods

The CPD technique was used to measure a number of mirror panels. Photogrammetry and flux mapping measurements were also conducted on the panels, to allow for a comparison of results.

The following sections cover the steps taken to make these measurements.

## 6.1. CPD Procedure

Each mirror panel to be measured was placed on the feet of the mirror frame, and held in place with the clamp at the top. The mirror surface was cleaned using glass cleaning spray and a cloth.

The bottom of the panel was pulled all the way out to the end of the feet. The glass at the top left corner of the mirror panel was lined up to be in the same plane as the locating disc. The clamp was used to hold the panel at this position, instead of adjusting the support bolts.

The orientation of the mirror panel was recorded by writing down where the ID label on the back of the panel is. It is either at the top, bottom, left or right, as looking at the front of the mirror frame.

The same camera (Nikon D300, with AF Nikkor 20mm 1:2.8 D lens) was used to perform all measurements, as was used to calibrate the coloured pattern in section 5.1.2.

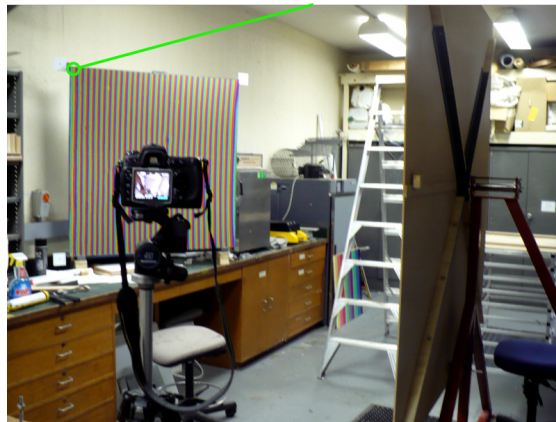


Figure 6.1.: Taking photograph of mirror panel surface. Top left corner of mirror panel is lined up so that it reflects the top right corner segment of the coloured pattern, as marked on image by green line.

## 6. Experimental Methods

The camera was attached to a tripod and positioned so that the top left corner of the mirror reflects the top right segment of the coloured pattern (see figure 6.1). Practice photos and the camera preview zoom function were used as an aid in lining up the corner. In some cases the left hand edge of the panel was badly warped, which made it difficult to line up the top corner while keeping the pattern reflection over the whole mirror surface. In these cases the panel was rotated so that a better mirror edge was on the left.

For most measurements the camera had the settings in table 6.1. If the image was under or over exposed then these settings were fine tuned. The camera was found to focus the reference dots at just over the 2m mark on the lens. This puts the mirror surface in focus, while the pattern reflection will be slightly out of focus (see appendix section B.3 for details). For standard panel measurements the camera was kept at this focus.

Table 6.1.: Camera settings.

Setting	Value
Image format	TIFF (non-lossy)
Image size	4288 × 2848
Colour	Natural (no sharpening)
White balance	Cool-white fluorescent
Aperture	8
Shutter speed	1/6s
ISO	250

The ambient temperature of the workshop area was recorded and then a photograph was taken. The pattern was then rotated 90° and locked into place and then a second photograph was taken. Care was taken not to move the camera between shots.

This process was then repeated for any other mirror panels that were measured, while keeping track of which photographs correspond to what mirror panels.

Once a set of mirror panels had their photographs taken, the photos were loaded onto a x86\_64 Linux laptop for processing. The image files were renamed to `id-orien-temp-rot.tiff`, where `id` is the mirror panel ID, `orien` is the orientation of the panel (label at either top, bottom, left or right), `temp` is the workshop temperature and `rot` is the rotation of the pattern for the photograph (segments either horizontally or vertically aligned).

An image viewing program was used to view one of the images for each mirror panel. The mouse was moved over each of the 3 reference dots, and their rough pixel locations were recorded. The `deflect.py` GUI could have been used to perform this task, but for debugging and experimenting, where the program was run multiple times for each panel, it saved time to create a batch script that directly called the program.

A total of 10 mirror panels were measured using this standard approach. A number of these panels were remeasured with altered measurement setups. This

## 6. Experimental Methods

was done to get an indication of the sensitivity of the process. The following aspects of the setup were changed:

- The camera focus.
- Photographs taken with mirror at far left and far right of image.
- Workshop lighting altered (see figure 6.2).
- Photographs taken in RAW image format, and then later converted to TIFFs.
- Mirror surface left dirty.



Figure 6.2.: Orange plastic placed over fluorescent light to change the lighting colour of the workshop.

## 6.2. Photogrammetry Measurements

Mirror panel photogrammetry measurements were taken to allow a comparison of RoCs, and calculated slope errors. 5 mirror panels were measured using the method outlined by Burgess et al. (2009). 3 of these measurements had already been performed by STG staff. Measurements of painted mirrored surfaces were favoured over those on the back of the panel.

## 6.3. Flux Mapping Measurements

4 mirror panel flux maps had been performed by STG staff. These allow a comparison of slope errors with the CPD measurements. The method outlined in section 3.2 was used to flux map mirror panels. The IDL program *dishfluxanalyser.pro*, written by Glen Johnston and Greg Burgess, was used to calculate slope errors from the photographs.

## *6. Experimental Methods*

### **6.4. Dial Gauge Measurements**

Dial gauge measurements as described in section 3.3, had been performed by STG staff on 5 of the mirror panels. These allow simple RoC comparisons where photogrammetry data is missing.

# 7. Results and Discussion

The first part of this chapter looks at the performance of the CPD method by comparing measured RoCs and slope errors to those obtained by photogrammetry and flux mapping. The second part investigates the error and sensitivity of the deflectometry measurements.

## 7.1. RoC Comparisons

Table 7.1 compares the RoCs measured for different mirror panels. Data from both photogrammetry and dial gauge measurements are included for comparison. The 3 larger RoC mirror panels are separated at the bottom of the table.

Information is given on the two principal RoCs as fitted by an elliptic paraboloid, and the geometric mean RoC. The percent difference between the deflectometry results and other techniques is also given.  $\phi$  is the angle between the mirror panel and the larger principal RoC  $R_1$ , as shown in figure 7.1. This value was calculated by using the z rotation data from the deflectometry result, and applying an offset depending on the orientation of the mirror as it was measured (bottom or top no offset, left or right 90° offset).

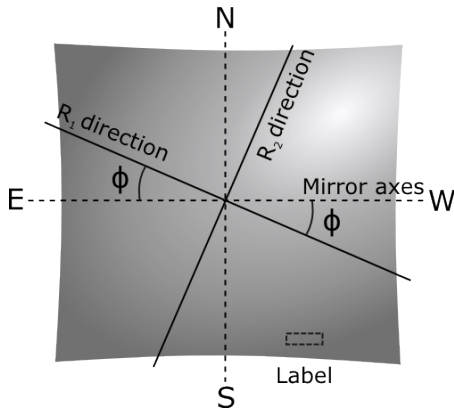


Figure 7.1.: A mirror panel has its edges labelled like a compass. Here the mirror panel ID label is on the back surface, at the bottom.  $\phi$  is the rotation of the principal direction  $R_1$ , relative to the E-W mirror axis.

Dial gauge measurements are only given where there is no photogrammetry data available. As discussed in section 3.3, dial gauge measurements can only be roughly compared, since they give inconsistent results, and don't necessarily give principal RoCs.

## 7. Results and Discussion

Photogrammetry on the other hand gives reliable RoC data. Typical mirror panel photogrammetry position measurements are accurate to within  $20\mu\text{m}$  in the z axis. In a worst case scenario all edge points could be off by around  $+20\mu\text{m}$ , and all centre points by  $-20\mu\text{m}$ . This would effectively change the depth of the panel by  $40\mu\text{m}$ . Using the depth to RoC equation (A.2), a 30m panel (depth of 5.704mm), would be measured as 29.79m. This is less than a 1% change. For a 85m RoC panel the error would be less than 2%.

Table 7.1.: RoC results. \* Photogrammetry was performed on front of panel. † 4 point dial gauge measurement. Suffix of deflect corresponds to the orientation of the panel as it was measured: b-bottom, t-top, l-left, r-right.

Panel ID	Method	$R_1$ (m)	% Diff	$R_2$ (m)	% Diff	$R_G$ (m)	% Diff	$\phi$ ( $^\circ$ )
411	deflec-b	29.80		27.17		28.45		24.14
	photo*	28.60	4.2	28.12	-3.4	28.36	0.3	115.00
373	deflec-b	37.69		33.17		35.36		21.36
	photo*	36.13	4.3	33.98	-2.4	35.03	0.9	29.33
247	deflec-t	34.01		28.40		31.08		-9.95
	photo	33.85	0.5	28.72	-1.1	31.18	-0.3	-4.88
040407	deflec-b	29.65		25.57		27.53		-15.10
	photo	28.97	2.4	25.85	-1.1	27.36	0.6	-5.74
037	deflec-t	33.15		30.32		31.71		-7.14
	dial†	32.65	1.5	27.53	10.1	29.98	5.8	0.00
035	deflec-r	31.17		25.65		28.28		-25.61
	dial	31.98	-2.5	22.37	14.6	26.75	5.7	0.00
210908	deflec-b	21.46		19.66		20.54		96.09
015	deflec-b	96.57		67.48		80.73		16.90
	photo	83.65	15.4	65.05	3.7	73.77	9.4	13.70
	dial	76.99	25.4	66.77	1.1	71.70	12.6	0.00
018	deflec-b	116.22		71.44		91.12		11.21
	dial	90.16	28.9	74.21	-3.7	81.80	11.4	0.00
019	deflec-b	114.80		83.77		98.06		2.12
	dial†	85.92	33.6	57.09	46.7	70.04	40.0	0.00

Figure 7.2 shows a plot of the RoCs calculated for the panels that had both deflectometry and photogrammetry measurements.

Deflectometry tends to overestimate  $R_1$ , and underestimate  $R_2$ , compared to the photogrammetry results. The smaller RoC panels are within 5% of the photogrammetry results. The large RoC panel 015 is however 15% off. The geometric means agree better, within 1% for smaller RoC panels and 10% for panel 015. These errors are not explained by the simulation analysis done in section 4.5. It showed that the error would be around 0.5% for a panel with RoC of 30m, with

## 7. Results and Discussion

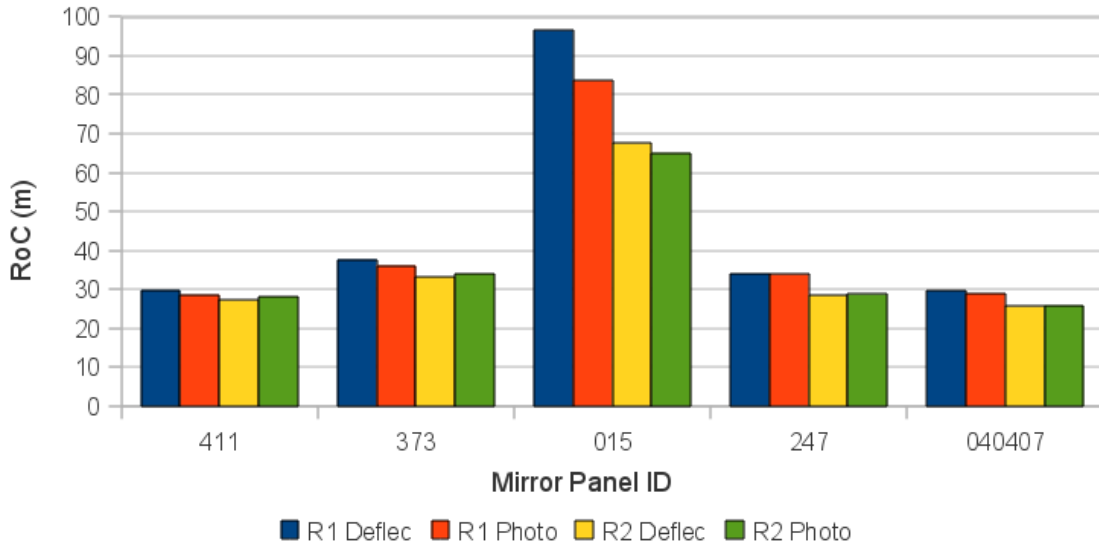


Figure 7.2.: Plot of principal RoCs for mirror panels measured with both deflectometry and photogrammetry.

an initial positioning depth error of 2mm.

It is worth mentioning that the RoC of large RoC mirror panels such as 015 is unstable. A small deflection of the panel or temperature change can cause a large change in RoC. Because of this it is difficult to make a judgement about how much of the error can be attributable to deflectometry, and how much to environmental changes impacting on the panel shape.

One thing to notice for the panel 411 measurement, is that the  $\phi$  rotation is almost exactly  $90^\circ$  out from that of photogrammetry. This, and many of the other discrepancies between the deflectometry and photogrammetry results, are due to a systematic error in the deflectometry method. This error will be discussed in section 7.3.

Figure 7.3 shows a 3D mesh plot of panel 210906 surface positions, output from deflectometry. This plot was created using gnuplot and the dgrid3d function.

## 7.2. Slope Error Comparisons

Table 7.2 compares the slope errors calculated from deflectometry, flux mapping and photogrammetry. The  $\sigma_1$  component of slope error is in the direction of the E-W panel axis.  $\sigma_2$  is the N-S component.

Neither of the flux mapping or photogrammetry slope errors are an ideal comparison. Photogrammetry gives slope errors for which the accuracy is unproven. Flux mapping slope errors are not calculated relative to the best fit surface like photogrammetry and deflectometry, but to a surface which depends on the measurement setup (see section 3.2). Because of this it is expected that deflectometry slope errors would be smaller than flux mapping slope errors.

## 7. Results and Discussion

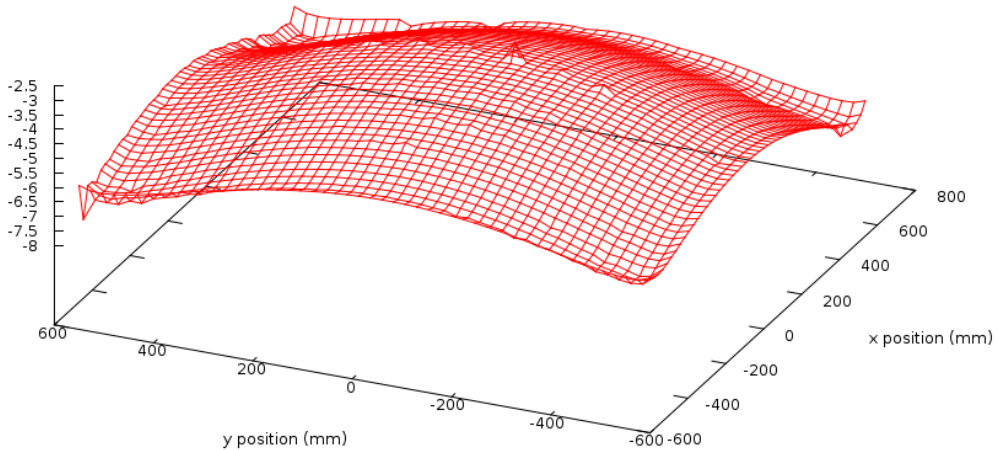


Figure 7.3.: 3D mesh of panel 210906 surface, with highly exaggerated z axis in mm. The closest corner is the top left corner of the mirror panel as it was measured. The edges of the panel can be seen to spring back from the rest of the panel shape which is an artefact of manufacturing process.

Table 7.2.: Slope error results for mirror panels.

Panel ID	Method	$\sigma_1$ (mrad)	% Diff	$\sigma_2$ (mrad)	% Diff
037	deflec-t	1.25		0.98	
	flux	1.15	8.4	1.13	-13.2
035	deflec-r	4.37		2.45	
	flux	4.67	-6.5	2.49	-1.3
040407	deflec-b	1.80		1.40	
	flux	1.34	34.1	1.33	5.3
	photo	1.06	69.6	0.92	52.2
210906	deflec-b	2.83		2.20	
	flux	2.80	1.1	2.50	-12.0
411	deflec-b	1.31		0.89	
	photo*	1.09	20.4	1.24	-27.9
373	deflec-b	1.18		0.81	
	photo*	0.95	23.7	1.25	-34.8
247	deflec-t	1.48		1.40	
	photo	1.00	48.2	0.97	44.3
015	deflec-b	1.03		0.81	
	photo	0.71	44.8	0.56	44.1
018	deflec-b	1.07		0.81	
019	deflec-b	1.24		1.08	

## 7. Results and Discussion

The slope errors agree well with the flux mapping, to within around 12%, that is except panel 040407. Panel 040407 has been in storage for around two years, stacked under the weight of other mirror panels, so might have become damaged in that time. It could be worthwhile flux mapping it again, to see if the slope error has indeed worsened as the deflectometry suggests.

Figure 7.4 shows the slope error distributions for panel 035. The plot is orientated so as viewed from the back of mirror panel, with the panel label on the top edge of the plot area. Panel 035 is a poor quality panel which has a large buckle in its shape. The effect of this buckle can be clearly seen in the slope error distributions.

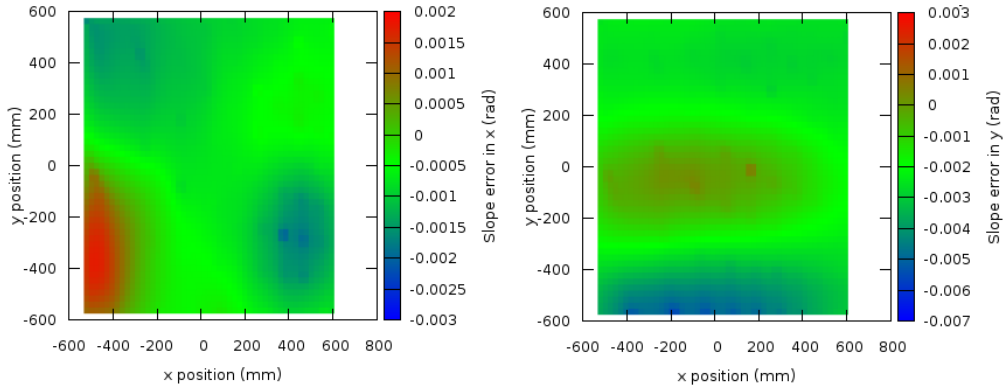


Figure 7.4.: Slope error plot for panel 035 with x component on left, and y component on right.

Figure 7.5 show the slope error distributions of panel 210906 which is another poor quality panel. However this panel has a rippled instead of buckled surface.

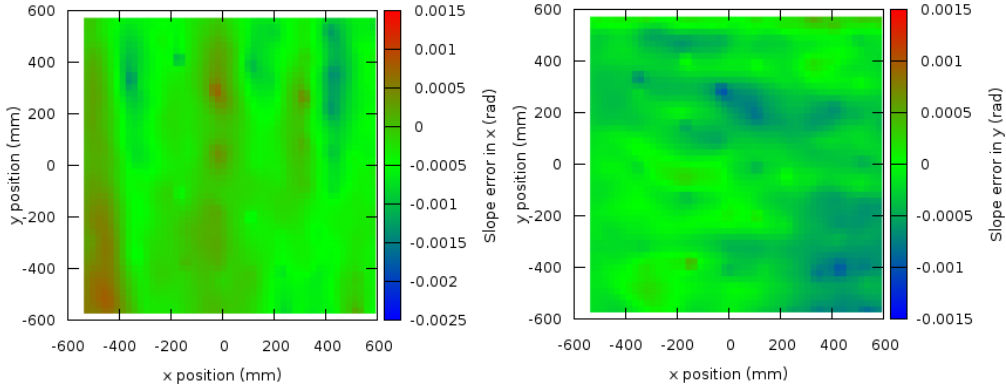


Figure 7.5.: Slope error plot for panel 210906 with x component on left, and y component on right.

While we can be quite confident in the RoCs measured from photogrammetry, it is different story for the flux mapping slope errors. A large sample of flux mapped mirror panels would be required to draw any definitive comparisons.

## 7. Results and Discussion

### 7.3. CPD Systematic Error

The fact that  $\phi$  for panel 411 is out by  $\sim 90^\circ$  from the photogrammetry results is a good indication that something is going wrong. Panels 411 and 373 were measured at all 4 orientations (b, t, l and r), in order to get a better insight into the discrepancy. The results are shown in table 7.3.

Table 7.3.: Measurements taken at different panel orientations. Suffix of deflect corresponds to the orientation of the panel as it was measured: b-bottom, t-top, l-left, r-right.

Panel ID	Method	$R_1$ (m)	$R_2$ (m)	$\phi$ ( $^\circ$ )	$\sigma_1$ (mrad)	$\sigma_2$ (mrad)
411	deflec-b	29.80	27.17	24.14	1.31	0.89
	deflec-t	30.76	27.58	10.39	1.32	1.01
	deflec-l	29.55	27.41	-68.14	1.09	0.95
	deflec-r	29.47	27.53	-64.34	1.09	0.96
373	deflec-b	37.69	33.17	21.36	1.18	0.81
	deflec-t	37.78	33.13	24.76	1.03	0.81
	deflec-l	36.86	34.03	-64.48	0.91	0.89
	deflec-r	36.52	34.28	-54.01	0.94	0.81

In both panels a trend is present where those measured with the label at the top or bottom produce a similar  $\phi$ , and those with the label at the left or right are similar. These two pairs of similar  $\phi$  are separated by  $\sim 90^\circ$ . If  $\phi$  were to be measured relative to the mirror frame, then these results would produce a constant value. This suggests that for these panels the principal RoCs are dependent on the measurement setup, not the shape of the panel itself.

To gain a greater understanding of this error, the deflectometry data points were directly compared to the photogrammetry points using the *comparesurfaces.pro* IDL program written by Greg Burgess. This program aligns the two datasets and then grids them. One surface is then subtracted from the other, and the difference is plotted.

The coordinate systems of the two methods are different, so the deflectometry measurements were converted to the photogrammetry coordinate system. This was done by either inverting and/or switching one or more of the coordinates within the program.

The difference surfaces for panels 411 and 015, measured with labels at the bottom, can be seen in figure 7.6. For this and every other difference surface image, the South mirror panel edge is the closest edge on the right, and the mirror surface faces up. The standard deviation of surface difference is better than 0.2mm for both surfaces. The difference surfaces for panel 411 measured at the other 3 orientations can be seen in figure 7.7.

The plots show an error that takes on the rough form of a hyperbolic paraboloid,

## 7. Results and Discussion

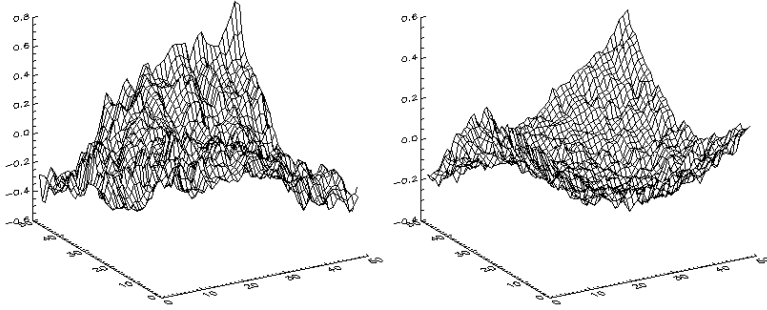


Figure 7.6.: Panel 411 (left) and 015 difference surfaces relative to photogrammetry. Note that the x and y axes correspond to bin numbers.

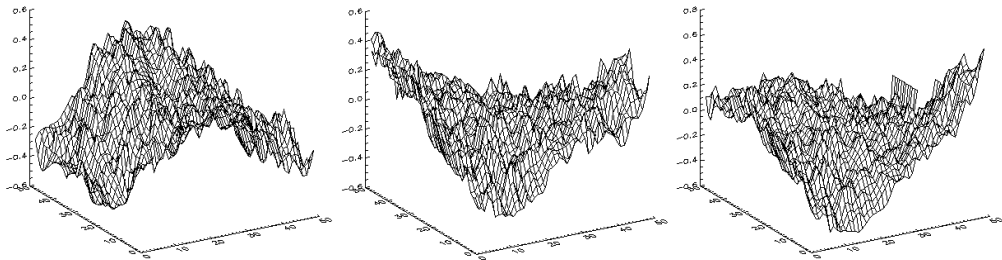


Figure 7.7.: Panel 411 difference surfaces. Left plot was measured with  $t$  orientation, centre plot with  $l$  orientation, and right plot with  $r$  orientation.

approximately aligned with the mirror diagonal. The fact that the same shape is repeated, demonstrates that this is not just a random error. The rotations of panel 411 show how this error stays stationary relative to the mirror panel frame, which is what the  $\phi$  values suggested.

The convex part of the error runs roughly along the mirror frame diagonal, from the top left corner of the frame, to the bottom right corner. The concave part is along the other diagonal. This is consistent with the resulting errors in the RoCs.  $R_1$  (the larger RoC) tends to run along the convex diagonal, and  $R_2$  along the concave one.

This explains the behaviour of panels 411 and 373 when rotated. These panels are both roughly spherical ( $R_1 \approx R_2$ ), therefore  $R_1$  will always appear near the convex diagonal.

For panels with a large enough difference between its principal RoCs,  $\phi$  should remain roughly the same for all orientations. In this case the panel RoCs are dominant, whereas in the previous case the error RoCs were dominant. Depending on the orientation the panel, the dominant panel RoCs will either line up with the convex or concave part of the error, or somewhere in between. Therefore one RoC is likely to increase while the other decreases.

There is the possibility that this error is an intrinsic part of the deflectometry method. Another possibility is that there is a simple mistake in the program code. This would have to be a subtle error since the results are close to what is expected.

## 7. Results and Discussion

The third possibility is that one or more calibration parameters are wrong.

The most likely part of the deflectometry method causing this error would be the way the surface positions are integrated up. While although the simulation performed to test this suggested a high accuracy, it was performed on a 1D curve, and it is not yet obvious whether or not this same accuracy carries through to the case of 2D surfaces.

The simplest way to check if this is the cause, is to move the starting point from the default top left corner of the mirror, to another location. If the error trend is observed to move with the starting point, then it is likely to be the cause. Table 7.4 shows the results for panel 411 using different starting locations.

The TL, TR and BL starting depths were measured roughly. The rest of the starting depths were chosen by using the mirror RoC to depth equation A.1, given the approximate RoC of the mirror panel.

Table 7.4.: Results for different panel 411 surface starting points. T-top, B-bottom, L-left, R-right, M-middle.

Panel ID	Method	$R_1$ (m)	$R_2$ (m)	$\phi$ ( $^{\circ}$ )	$\sigma_1$ (mrad)	$\sigma_2$ (mrad)
411	deflec-b TL	30.29	27.24	27.44	1.33	0.89
	deflec-b BL	29.86	27.36	60.62	1.05	0.98
	deflec-b BR	30.46	26.23	23.26	1.40	1.00
	deflec-b TR	31.13	26.84	65.79	1.16	1.19
	deflec-b ML	30.95	27.03	45.86	1.25	0.80
	deflec-b MM	30.12	27.44	43.24	1.17	0.88

The results show how  $\phi$  is roughly the same for starting points diagonally opposite to one another. However the difference is only about  $40^{\circ}$  between neighbouring corner schemes, not the  $90^{\circ}$  expected if the error follows the starting point. Difference surfaces were plotted between these results and the photogrammetry to better observe how the error changes. The results for 3 of these plots can be seen in figure 7.8.

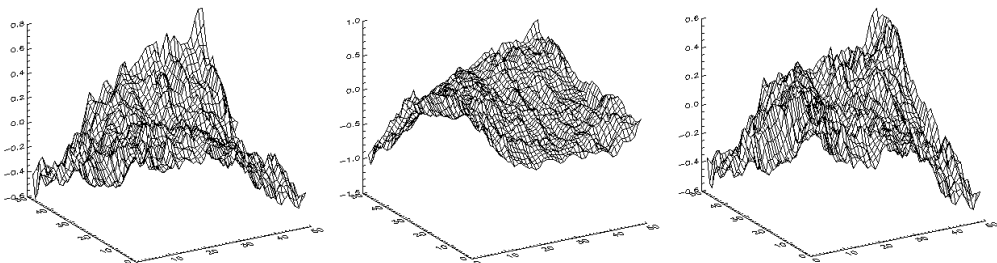


Figure 7.8.: Panel 411 difference surfaces. Left plot uses the top left as a starting point, the centre plot uses top right, and the right plot uses the centre of the panel.

## 7. Results and Discussion

The shape of the error changes somewhat in these plots, but the orientation does not follow the error. Overall these results suggest that the surface integration might have a part to play in this systematic error, but it is not the sole cause. The search for the source of the error continues in the following section.

This systematic error has an effect on the calculated slopes as well as RoCs. Assume that the error causes a local offset of 1.0mm from the measured surface. The change in calculated slope for this offset area would be  $\sim 0.25\text{mrad}$  (using equation A.4). This will have an impact on the slope errors calculated for the surface. Slope errors also changed in another way. They are calculated relative to the fitted surface, which depends on the systematic error.

## 7.4. Sensitivity Analysis

The results for the measurements made under different setup conditions (see section 6.1), are shown in table 7.5.

Table 7.5.: Percent change in deflectometry measurements, for changed measurement setup.

Panel ID	Method	$\Delta R_1$ (%)	$\Delta R_2$ (%)	$\Delta\phi$ (%)	$\Delta\sigma_1$ (%)	$\Delta\sigma_2$ (%)
411	f=inf	2.5	0.8	12.7	6.2	2.5
	f=1	-2.4	-3.1	14.0	0.8	-1.9
	f=0.7	-5.1	-5.5	6.9	2.8	0.3
	left	-1.2	-1.4	37.6	-14.2	-11.7
	right	-0.6	-2.7	-12.8	10.3	6.5
	orange	1.8	0.3	2.4	6.3	5.7
	373	0.0	-0.3	-3.2	0.3	1.4
210906	dirty	0.1	-0.6	26.5	0.4	0.1

Changing the focus has quite a significant effect on the results. This is thought to be in part due to the fact that the principal distance in the program was not also changed to match the focus. A badly out of focus image may also make it more difficult to centroid the reference dots, which will in turn cause the camera to be poorly positioned.

The simple act of taking the mirror panel measurement photographs off centre has a rather significant effect on the slope error and  $\phi$  results. Such a large change was not expected since the obvious cause, radial lens distortion (see appendix section B.2), has been corrected for. It is strange to note that both  $\sigma_1$  and  $\sigma_2$  change, and this change has a trend to it. It is definitely worth further investigating the cause of this error, and whether or not it is tied to the mirror shape systematic error.

The changed lighting conditions have a larger effect on the slope error outcome than the RoCs. This is because changing the ambient lighting colour without

## 7. Results and Discussion

changing the calibration file, will cause the program to relate hue positions to the wrong position within a pattern segment. Because this is only happening on the scale of a segment, the overall shape of the mirror is hardly effected, but errors on a small scale will be created, hence the increase in slope error.

The RAW file hardly changes the outcome, demonstrating that the pixel pairing effect present in camera TIFFs can be ignored.

The dirty mirror measurement strangely only significantly affects  $\phi$ . It was anticipated that the slope error of the panel would change more. However panel 210906 is already a poor quality panel, so slope error might be more effected for a good quality panel.

These results indicate that the setup conditions need to be fine tuned to produce measurements that best represent the actual mirror panel surface. Once these conditions are found, the setup needs to be controlled in order to produce consistent results.

To form an even broader picture of the method sensitivity, a number of program calibration parameters were altered, and then the program was rerun on mirror panel 411. This analysis was also performed to check if a specific calibration setting is responsible for the systematic error discussed in section 7.3.

Both of panel 411's RoCs are close to one another according to photogrammetry. The deflectometry systematic error causes one RoC to increase, and the other to decrease. Therefore any beneficial change in a parameter would bring both RoCs closer to one another (i.e. decrease in  $R_1$  and increase in  $R_2$ ).

The description of the parameters that were changed are given below, and the results can be seen in table 7.6.

**pxsize** Camera pixel size.

**prdist** Camera principal distance.

**sopc** Camera sensor optical centre position.

**patxoff** Segment x offset from coloured pattern corner.

**patyoff** Segment y offset from coloured pattern corner.

**segsize** Size of coloured pattern segment.

**startdepth** Starting depth of first point on mirror.

Increasing the sensor optical sensor x position was the only change that reduced the effects of the systematic error. Even then the change was minimal. Increasing the parameter further resulted in no more significant benefits, and eventually a worse result. All other parameter changes either increase the gap between the RoCs, or shift them up and down together.

Additional program parameters such as camera position, coloured pattern global position and coloured pattern transformation matrix were altered, but all were found to cause no significant beneficial changes to the systematic error.

## 7. Results and Discussion

Table 7.6.: Percent change in panel 411 deflectometry results, for change in parameters.

Parameter	Change (mm)	$\Delta R_1$ (%)	$\Delta R_2$ (%)	$\Delta\phi$ (%)	$\Delta\sigma_1$ (%)	$\Delta\sigma_2$ (%)
pxsize	0.0001	-8.1	-6.7	-1.6	-12.4	-8.3
pxsize	-0.0001	10.6	8.2	-2.1	5.1	10.4
prdist	0.1	2.9	2.2	-2.8	-2.2	2.1
prdist	-0.1	-2.1	-1.7	-3.3	-6.9	-3.1
soptc x	0.2	-0.2	0.6	10.1	-10.4	-5.9
soptc x	-0.2	0.9	-0.3	-12.1	1.4	5.9
soptc y	0.2	1.1	1.5	4.6	-9.1	-5.2
soptc y	-0.2	-0.5	-1.1	-9.3	0.8	5.6
patxoff	2	0.4	0.3	-5.2	-4.9	-0.2
patxoff	-2	0.2	0.1	-0.1	-4.9	-1.1
patyoff	2	0.6	-0.1	-9.7	-1.0	5.0
patyoff	-2	0.1	0.4	5.9	-8.5	-6.0
segsize	0.05	1.7	1.0	-4.2	-2.7	1.8
segsize	-0.05	-1.0	-0.7	-0.4	-6.8	-3.2
startdepth	1	-0.1	-0.1	-2.5	-4.9	-0.7
startdepth	-1	0.7	0.5	-1.9	-4.8	-0.9

It could be that a series of parameters, such as segment size, pattern position, principal point and focus all contribute to the error. However there are too many parameters to thoroughly test this idea.

All measurements were made at an ambient temperature of around 15°C ( $\pm 1^\circ\text{C}$ ). A change in ambient temperature can have an effect on panel RoC. Using equation A.3, the change in RoC for a 30m panel between 15°C and 16°C is approximately  $-0.13\text{m}$ , or less than 0.5%. This change is swamped by the effect of the systematic error, so the correction was omitted for all RoC calculations.

Gravity does change the shape of the mirror panel, however this is minimal when the panel is sitting vertical on its edge. This is the same way a panel sits during photogrammetry measurements.

## 7.5. Improvements

It is disappointing that an unforeseen systematic error is reducing the accuracy of the method. The source of the error would be discovered if given more time to perform tests on the method. One such test would involve running controlled dummy data through the program. This controlled data could be analysed as it is processed at different steps in the program. The question still remains if the error can be fixed once the source is discovered.

## *7. Results and Discussion*

If the error is found to be an intrinsic part of method, then it might instead be possible to account for it. For example the hyperbolic shape of the error could be modelled. It could then be subtracted away from surface position measurements, before a curve is fit to it. This would likely only work under certain conditions such as a limited range of mirror panel RoCs, but it could still be useful.

There is a better approach to test the accuracy of mirror panel slope errors, than comparison to flux mapping slope errors. The idea is to ray trace the surface solved by deflectometry. Given the right setup, the results could then be directly compared to flux mapping flux distributions. In order to ray trace the surface, a custom program would have to likely be programmed.

## 8. Conclusion

This thesis aimed to design and demonstrate a new method of measuring the RoCs and slope errors of a mirror panel. The coloured pattern deflectometry method was developed with the requirements of low cost, speed and simplicity in mind.

For smaller RoC panels ( $\sim 30\text{m}$ ) the RoCs agree to within 5% of photogrammetry measurements. Unfortunately the orientation of these principal RoCs cannot be relied upon for almost spherical mirror panels. Geometric mean RoCs were found to produce more reliable results, to within 1% of the photogrammetry. For larger RoC mirror panels, of the order of 100m, the errors become much worse.

Initial slope error measurements prove promising, however for more definitive results, a more direct comparison is needed than that made with flux mapping data.

The deflectometry results were found to be quite sensitive to the measurement setup. Therefore a semi-controlled environment is required to produce consistent results.

Photogrammetry is still superior in terms of producing accurate principal RoC measurements. If geometric mean RoCs are all that is required, then the CPD method is on par with photogrammetry in terms of accuracy for  $\sim 30\text{m}$  RoC panels. The deflectometry system provides more detailed and accurate slope error results, and is also much faster (4-6mins instead of 15-20mins).

From initial results it appears that the deflectometry is at least just as reliable as flux mapping at providing slope errors. However further testing is required to actually determine the accuracy of the slope errors produced. The CPD method has a number of benefits over flux mapping. It is much faster, does not depend on the weather or time of day, and gives the distribution of slope errors over the panel surface.

Compared to QualiSURF this method does not produce as high slope resolutions, but it provides valuable mirror panel RoC and surface position data.

The key way of improving on this method would be to eliminate the systematic error found in the surface position results. With further experimentation and testing, there is a high chance that the source of the systematic error could be established, and given enough time, its effects removed. This would bring the method into a much more useable state.

# Appendices

# A. Mirror Panel Equations

## A.1. Depth to RoC Approximation

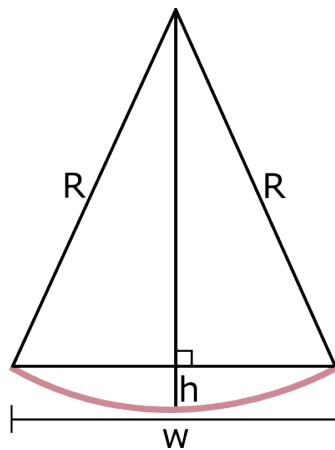


Figure A.1.: Relationship between the depth of a spherical mirror panel and its RoC.

The relation between the depth of a spherical mirror panel and its RoC is given by:

$$h = R - \sqrt{R^2 - (w/2)^2} \quad (\text{A.1})$$

Solving for the RoC we get:

$$R = \frac{(w/2)^2 + d^2}{2d} \quad (\text{A.2})$$

## A.2. Temperature Effects

For mirror panel supported horizontally with a RoC of around 30m, the following temperature trend has been observed by the STG:

$$R_T \approx R_{T_0} - 0.13(T - T_0) \quad (\text{A.3})$$

### A. Mirror Panel Equations

## A.3. Offset Slope Error

Calculating the slope of a mirror point at a location offset by  $h$  from the actual mirror, causes an error in slope. This error is calculated with the aid of figure A.2.

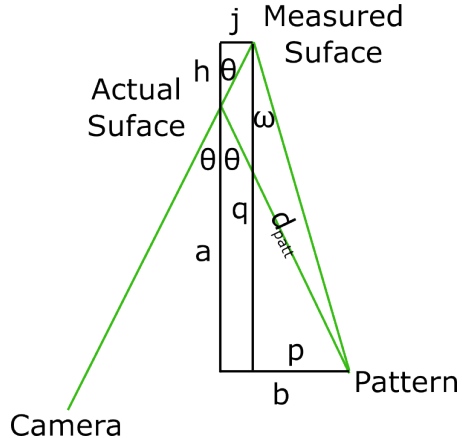


Figure A.2.: Relationship between the depth of a spherical mirror panel and its RoC.

The change in slope is given by:

$$\Delta\theta = \frac{\omega - \theta}{2} \quad (\text{A.4})$$

where  $\omega$  can be calculated from:

$$\omega = \tan^{-1} \left( \frac{p}{q} \right) \quad (\text{A.5})$$

$$p = b - j = d_{patt} \sin \theta - h \tan \theta \quad (\text{A.6})$$

$$q = a + h = d_{patt} \cos \theta + h \quad (\text{A.7})$$

## B. Camera and Lens Optics

Digital cameras are a useful measurement tool because they are cheap and can capture a lot of information in just one photograph. In order to use a camera for this purpose it is essential to understand the underlying optics of a camera, starting with the optics of a lens.

### B.1. Lens Cardinal Points

The behaviour of a lens is best understood by describing it with a set of cardinal points.

The optical axis of a lens is the path that a light ray can take through a lens without being refracted. A ray will travel along the optical axis as if the lens wasn't there (apart from a temporary slowing down in the lens medium). This is often equal to the axis of rotational symmetry, and is normal to the front and back surface radii of curvature for a simple lens.

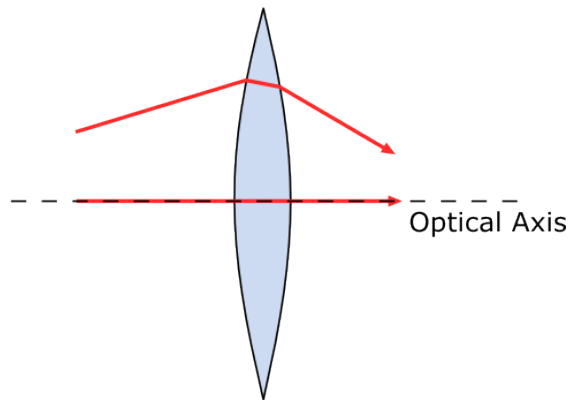


Figure B.1.: Optical axis of a simple convex lens. Rays striking the lens will be refracted if they aren't on the optical axis.

If light rays enter a lens parallel to the optical axis, they will converge at the focal point of the lens (see figure B.2). This is the first of the cardinal points. A lens has two focal points, one for when light enters the lens from the left and the other for when it enters from the right.

The distance of a light ray from the optical axis as it crosses the first principal surface will be the same distance when it passes through the second principal surface. The lens can then be simplified by ignoring what happens between these surfaces and saying light is refracted only once as it exits the second surface. The

## B. Camera and Lens Optics

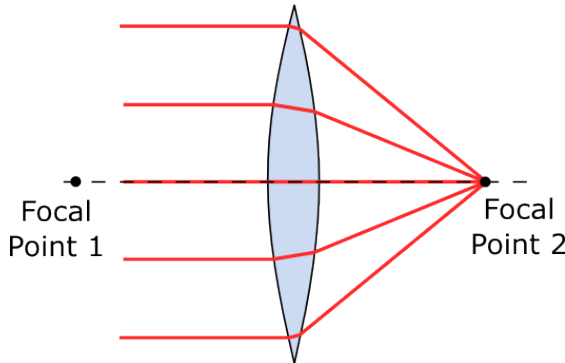


Figure B.2.: Focal points of lens.

principal points of the lens correspond to where the optical axis intersects with these principal surfaces.

The nodal points are the unique points where any ray aimed at the first nodal point before it enters the lens, will exit the lens as if it had originated from the second nodal point, parallel to its entering ray.

For a lens system where the first medium has the same index of refraction as the second medium, the principal and nodal points will coincide. This is the case for a camera.

A further simplification can be made for a thin lens. The thin lens approximation assumes that all principal and nodal points coincide at the centre of the lens.

The effective focal length (EFL) is the distance from the second principal point to the second focal point. This is the distance from the second principal point to the capture array (CCD array or equivalent) for a digital camera focused at infinity.

Focusing a camera on an object closer than infinity moves the capture array away from the lens a small amount. The distance between the capture array and the second principal point is known as the principal distance. The principal distance and focal length are equivalent for a camera focused at infinity.

## B.2. Radial Lens Distortion

The distorted radius  $r_d$  is often modelled as being related to the actual radius  $r$  by a polynomial such as:

$$r_d = r + k_1 r^3 + k_2 r^5 + \dots \quad (\text{B.1})$$

Usually only odd powers are used since they are easier to calibrate (Das & Patil 2006). Photogrammetry often uses just the first 2 or 3 terms to model the radial distortion.

This equation can be used to construct an undistorted image from existing pixels, by moving to a radius  $r$  and giving it a pixel value equal to what was measured

## B. Camera and Lens Optics

at  $r_d$ . However if we just want to find the undistorted position of a distorted pixel, then we need the inverse of this equation. The radial distortion model to 2 terms ( $k_1$  and  $k_2$ ) does not have an exact analytical inverse, but it can be approximated for small distortions by (Ma et al. (2003) and Ghosh (2005)):

$$r = r_d - k_1 r_d^3 - k_2 r_d^5 \quad (\text{B.2})$$

In terms of the camera sensor x and y components this equation becomes:

$$x = x_d(1 - k_1 r_d^2 - k_2 r_d^4) \quad (\text{B.3})$$

$$y = y_d(1 - k_1 r_d^2 - k_2 r_d^4) \quad (\text{B.4})$$

## B.3. Focusing on Mirrored Surface

As discussed in section 4.2 there are a number different paths light takes within a camera, to end up at a given pixel. When a camera is used to photograph a mirrored surface, things get a bit more complicated. When photographing a mirror panel the question arises of whether the mirror surface should be in focus, or the coloured pattern should be in focus. Figures B.3 and B.4 qualitatively show these two possibilities.

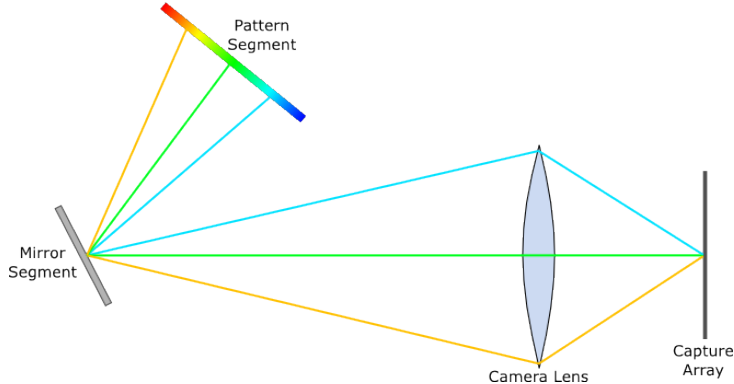


Figure B.3.: Camera focused on mirrored surface.

A range of hue values will be received by any given pixel if the camera is focused on the mirror surface. However these hues tend to cancel out to produce the hue that enters the nodal points of the lens (yellow and blue give green). The effect of focussing on the pattern is to reduce the mirrored surface resolution. A finite surface spot is now being measured. Both of these effects depend on the aperture of the camera. A larger F value will reduce both of these errors.

## B. Camera and Lens Optics

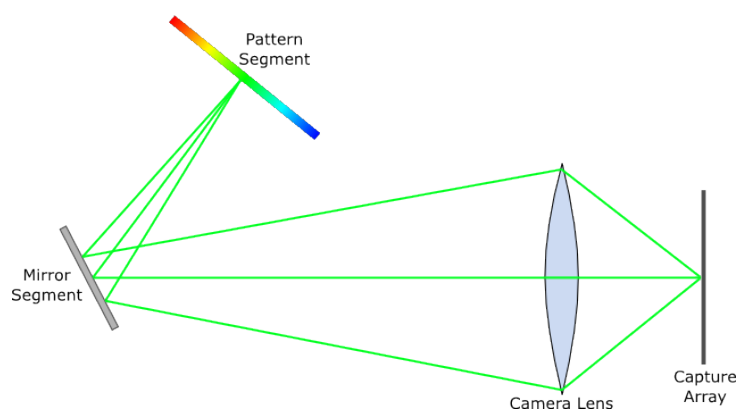


Figure B.4.: Camera focused on coloured pattern.

# Bibliography

- Burgess, G. & Lovegrove, K. (2007), Optics of dish concentrators. ANU Solar Thermal Group draft internal technical report, v0.4.
- Burgess, G., Shortis, M. R., Kearton, A. & Garzoli, J. (2009), Photogrammetry for dish construction, *in* ‘Solar09, 46th ANZSES Conference’, Townsville, Queensland, Australia.
- Butler, B. L. & Pettit, R. B. (1977), Optical evaluation techniques for reflecting solar concentrators, *in* ‘Vol. 114 Optics Applied to Solar Energy Conversion’, SPIE.
- Das, A. & Patil, D. (2006), ‘Efficient measurement and correction techniques for lens distortion’, <http://scien.stanford.edu/class/psych221/projects/06/ddpatil/ee362ProjectReport.pdf> [Accessed Sept 2009]. EE362 Final Project, Stanford Center for Image Systems Engineering.
- Fernholz, K., Hsakou, R., Lazarz, K., Wang, C. S., Emerson, B., Biernat, D. & Case, D. (2007), Development of a tool to measure bond-line read-through defects, *in* ‘Proceedings of 7th-Annual Automotive Composites Conference and Exposition / Society of Plastics Engineers’.
- Ghosh, S. K. (2005), *Fundamentals of Computational Photogrammetry*, Concept Publishing Company.
- Harris, J. A. & Duff, W. S. (1981), ‘Focal plane flux distributions produced by solar concentrating reflectors’, *Solar Energy* **27**, 403–411.
- Johnston, G. (1995), ‘On the analysis of surface error distributions on concentrated solar collectors’, *Journal of Solar Energy Engineering* **11**, 294–296.
- Johnston, G., Lovegrove, K. & Luzzi, A. (2003), ‘Optical performance of spherical reflecting elements for use with paraboloidal dish concentrators’, *Solar Energy* **74**, 133–140.
- Kammel, S. & Puente León, F. (2005), Deflectometric measurement of specular surfaces, *in* ‘Instrumentation and Measurement Technology Conference 2005’, Ottawa, Ontario, Canada.
- Kohlenbach, P., McEvoy, S., Stein, W., Burton, A., Wong, K., Lovegrove, K., Burgess, G., Joe, W. & Coventry, J. (2007), Novel parabolic trough collectors

## Bibliography

- driving a small-scale organic rankine cycle system, in ‘Proceedings of the ASME Energy Sustainability Conference’, Long Beach, California, pp. 995–1003.
- Ma, L., Chen, Y. & Moore, K. L. (2003), ‘A new analytical radial distortion model for camera calibration’, *CoRR cs.CV/0307046*. <http://arXiv:cs/0307046v1> [cs.CV].
- Pettit, R. B. (1977), ‘Characterisation of the reflected beam profile of solar mirror materials’, *Solar Energy* **19**.
- Pottler, K., Lüpfert, E., Johnston, G. H. & Shortis, M. R. (2005), ‘Photogrammetry: A powerful tool for geometric analysis of solar concentrators and their components’, *Journal of Solar Energy Engineering* **127**, 94–101.
- Ulmer, S., Heinz, B., Pottler, K. & Lüpfert, E. (2009), ‘Slope error measurements of parabolic troughs using the reflected image of the absorber tube’, *Journal of Solar Energy Engineering* **131**.
- Ulmer, S., Heller, P. & Reinalter, W. (2008), ‘Slope measurements of parabolic dish concentrators using color-coded targets’, *Journal of Solar Energy Engineering* **130**.
- Weisstein, E. W. (n.d.a), ‘Curvature’, From MathWorld—A Wolfram Web Resource. <http://mathworld.wolfram.com/Curvature.html> [Accessed Sept 2009].
- Weisstein, E. W. (n.d.b), ‘Principal radius of curvature’, From MathWorld—A Wolfram Web Resource. <http://mathworld.wolfram.com/PrincipalRadiusofCurvature.html> [Accessed Sept 2009].